Carbon 200 (2022) 134–148

Contents lists available at ScienceDirect

Carbon

journal homepage: www.elsevier.com/locate/carbon

Highly porous and conductive functional carbon fibers from electrospun phosphorus-containing lignin fibers

Francisco J. García-Mateos, Juana M. Rosas, Ramiro Ruiz-Rosas, José Rodríguez-Mirasol *, Tomás Cordero

Universidad de Málaga, Departamento de Ingeniería Química, Andalucía Tech., Escuela de Ingenierías Industriales, Campus de Teatinos s/n, 29010, Málaga, Spain

ARTICLE INFO

Keywords:
Electrospinning
Lignin fiber
Phosphorus
Carbon fiber
Curved graphitic structures

ABSTRACT

Functional carbon fibers were prepared by carbonization of thermostabilized electrospun lignin-fibers at 500–900 °C followed by a high temperature thermal treatment at 1200–1600 °C. The effect of the preparation temperature on their surface chemistry, structural order, textural properties and electrochemical behavior has been stablished. Maximum porosity development is obtained at 900 °C. The addition of phosphoric acid in the electrospinning lignin solution shortens the stabilization time of the fibers, increases the carbonization yield, generates phosphorus functional groups (P content as high as 3% wt.) and increases the BET surface area of carbon fibers from 840 to 1143 $m^2 g^{-1}$. Interestingly, when phosphorus-containing carbon fibers are treated even at very high temperature, 1600 °C, most of the porosity is preserved (A_{BET} = 822 $m^2 g^{-1}$). XPS depth profile reveals the presence of reduced phosphorus in the core of carbonized fibers. XRD and TEM analysis make evident that the presence of phosphorus induces curvature of the graphitic layers, which seems to hinder the stacking of the graphene layers, explaining the preservation of microporosity after the thermal treatment at high temperature. However, Raman and XRD analyses point out that the presence of phosphorus does not affect the lateral growing of the crystallites. Thus, phosphorus preserves the porosity and allows the development of the electrical conductivity after the thermal treatments. Gravimetric capacitances of 79 F g^{-1} and capacitance retention of 63% at 68 A g^{-1} have been determined for phosphorus-containing carbon fibers prepared at 1200 °C.

1. Introduction

Lignin is one of the major components of the cell walls and one of the most abundant biopolymers on Earth. It is obtained at large amounts in pulp and paper industries through different processes, being Kraft pulping the most implemented process. In spite of being considered as a potential feedstock for the production of fine chemicals and materials [1,2], most of the produced lignin is consumed as a fuel in the pulp–-paper industry to recover energy and chemical reactant, and only a 2% of the produced lignin is actually being commercialized [3,4]. However, new processes like Organosolv one produces a type of lignin with very low amount of impurities. In this sense, the Alcell® pulping process (the most well-known process in the organosolv lignin category) exhibits higher pulp yields than the Kraft process and it is also more environmentally friendly [5]. Within a biorefinery scheme, large amounts of organosolv lignin are expected to be generated in future wood-to-ethanol bio-refineries. Therefore, the development of value-added lignin-based sustainable products will be decisive to the economic success of the bio-ethanol production by this process, also having an important impact on strengthening the transition towards the circular economy.

In this regard, the carbon-rich and high aromatic content of lignin structure turns it a promising raw precursor for the preparation of carbon materials [6,7]. Following this premise, we have reported the preparation of carbon molecular sieves, activated carbons, hierarchical porous carbons, carbon fibers and high temperature carbons from lignin [8–12]. More specifically, the production of carbon fibers from low-cost and abundant precursors like lignin could be an interesting alternative for its valorization, from both economic and environmental points of view [3,13]. According to their applications, carbon fibers can be classified into two different blocks: one related to the mechanical properties for structural applications; and another for functional applications, in

* Corresponding author. Universidad de Málaga, Departamento de Ingeniería Química, Andalucía Tech, Escuela de Ingeniería Industriales, Campus de Teatinos s/n, 29010, Málaga, Spain.
E-mail address: mirasol@uma.es (J. Rodríguez-Mirasol).

https://doi.org/10.1016/j.carbon.2022.08.050
Received 19 May 2022; Received in revised form 25 July 2022; Accepted 13 August 2022
Available online 16 August 2022

which some other properties such as high surface area, an adequate pore size and surface chemistry, high electrical conductivity, and elevated oxidation resistance are considered of great relevance.

In both cases, some post-treatments are required to optimize the fiber properties. In particular, heat treatment from 1500 up to 3000 °C becomes necessary to enhance the structural carbon order of the fibers, which improves the electrical conductivity and oxidation resistance. In this sense, some authors have reported the existence of a heterogeneous fine structure with inclusions of a highly graphitized nature in lignin-based carbon fibers treated at 1500 °C [14]. Baker and Gallego found an increase of the graphitization with lignin-derived carbon fibers treated up to 2700 °C [15]. Evidences for this effect at high temperature treatment on the structural order of the final carbon was also reported by Rodriguez-Mirasol et al. for lignin powder treated at temperatures as high as 2800 °C [12], and by Compere et al. for soda harwood lignin-poly(ethylene) terephthalate treated at 1200 °C [16].

However, an improvement of the structural order of carbon material by thermal treatment at high temperatures conduces irrevocably to a large decrease of the porosity and the surface area, which represents a strong drawback for some functional applications, such as in electrochemical-related ones. Therefore, the optimization of the post-treatment of the carbon fibers with the goal of increasing both the structural ordering and the porosity development is an important challenge.

With regard to the preparation method, in previous works, we have reported the preparation of lignin-derived carbon fibers by means of a simple and versatile technique, such as electrospinning, without the incorporation of any spinning-assisted agent, reducing the manufacture complexity, time and costs [11,17–22]. Electrospun lignin-based carbon nanofibers are receiving a growing interest for energy conversion and storage application owing to their improved electrical and ion transfer and the presence of microporosity [21,23–26]. Moreover, we found that the addition of H_3PO_4 into the initial lignin solution shortens the stabilization process and produces more oxidized spun lignin fibers, due to the reaction of phosphoric acid with the dissolved lignin. This phosphoric acid generates phosphate (and/or polyphosphate) esters, which promote cross-linking into the lignin structure, increasing the glass transition temperature of the lignin, and so, reducing the time needed for the stabilization step. Moreover, it also produces lignin-fibers with a higher development of the porosity, oxidation resistance, together with a rich variety of P and O surface functionalities [22].

In this sense, the objective of this work is the preparation of porous and highly conductive carbon fibers from Alcell lignin by electrospinning. For this purpose, the influence of i) the addition of phosphoric acid in the initial solution, ii) the carbonization temperature, and iii) the heat treatment at temperatures from 1200 to 1600 °C on the surface chemistry, porosity, structural ordering, electrical conductivity and electrochemical performance of the carbon fibers is deeply studied.

2. Materials and methods

2.1. Preparation of carbon fibers

Carbon fibers were prepared by carbonization of electrospun lignin fibers using Alcell lignin as raw material. For the preparation of pure lignin fibers, a solution of lignin and ethanol, in a weight ratio of 1/1, was electrospun. Phosphorus-containing lignin fibers were obtained by electrospinning of H_3PO_4 (85%)/lignin/ethanol solutions, where two different H_3PO_4 to lignin mass ratio, 0.1/1/1 and 0.3/1/1, were used for their formulation. All solutions were stirred overnight at 200 rpm and 60 °C before spinning. A coaxial electrospinning setup was used for the spinning of the aforementioned lignin solutions. This device is described in detail elsewhere [17,20]. The aforementioned lignin solutions were feed to the device through the inner needle, while pure ethanol was pumped into the outer needle. The applied electrical potential differences were 14 kV for pure and lignin fibers with the low H_3PO_4 to lignin mass ratio (0.1/1/1 mass ratio) and 22 kV were applied for lignin fibers with high H_3PO_4 to lignin mass ratio (0.3/1/1 mass ratio). The tip-to-collector distance was 25 cm. Flow rate of 1 mL h^{-1} was set for the pure lignin and low H_3PO_4 to lignin mass ratio solutions, while the high H_3PO_4 to lignin mass ratio solution required an increase of the flow rate to 3 mL h^{-1} in order to achieve steady electrospinning regime. In all the cases, the pure ethanol flow rate through the outer needle was set to 10% of the flow rate of the lignin solution.

The obtained fibers were air stabilized (flow rate of 50 cm^3 min^{-1} STP) in a conventional oven. The stabilization was carried out from room temperature to 200 °C. On the one hand, for pure lignin fibers, the heating rate in the stabilization step was 0.08 °C min^{-1} and the final temperature was kept for 80 h. On the other hand, the stabilization step for phosphorus-containing lignin fibers (both H_3PO_4 to lignin mass ratios) was carried out at 0.8 °C min^{-1} and the final temperature was kept for 1 h. More details of the preparation method can be found elsewhere [20].

Stabilized fibers were carbonized in a tubular furnace at 500, 700 and 900 °C under a continuous flow of N_2 (150 cm^3 STP min^{-1}), with a heating rate of 10 °C min^{-1}. Pure carbon fibers (CFs) were directly stored for further use, whereas phosphorus-functionalized carbon fibers (PCFs) were washed with distilled water at 60 °C before storage. The carbon fibers prepared at 900 °C were also thermally treated at 1200, 1400 and 1600 °C for 1 h (heating rate of 5 °C min^{-1}, N_2 flow rate of 200 cm^3 STP min^{-1}) [27,28]. The nomenclature used in this work is CF and PCF for pure and phosphorus-functionalized carbon fibers, respectively. For PCFs, the acronym L, for the lowest H_3PO_4 to lignin mass ratio (0.1), or H, for the highest H_3PO_4 to lignin mass ratio of 0.3, was added at the end of the name. The final preparation temperatures were also included. For instance, the sample PCFL1200, makes reference to phosphorus-containing carbon fibers with an H_3PO_4 to lignin mass ratio of 0.1, obtained at 900 °C and followed by a thermal treatment at 1200 °C.

2.2. Characterization of carbon fibers

Ultimate analysis of the carbon fibers was carried out in a Leco CHNS-932 system, being the oxygen content calculated by difference. The surface chemistry of the sample was analyzed by X-ray photoelectron spectroscopy (5700C model Physical Electronics) with Mg kα radiation (1253.6 eV). The maximum of the C1s peak was set to 284.5 eV and used as reference for shifting the whole spectrum. Total amount of phosphorus of PCFH samples was determined by inductively coupled plasma optical emission spectrometry (ICP-OES). Temperature-programmed desorption (TPD) analyses were obtained in a customized quartz fixed-bed reactor placed inside an electrical furnace and coupled to both a mass spectrometer (Pfeiffer Omnistar GSD-301) and to a non-dispersive infrared (NDIR) gas analyzers (Siemens ULTRAMAT 22), in order to quantify CO and CO_2 evolution, (calibration error <1%). In these experiments, c. a. 50 mg of the carbon fibers was heated from room temperature to 930 °C, at a heating rate of 10 °C min^{-1}, in nitrogen (purity 99.999%, Air Liquide) flow (200 cm^3 STP min^{-1}). SEM images of the carbon fibers were obtained from a JSM 6490LV JEOL instrument and TEM images were obtained by using a Philips CM200 microscope (at an accelerating voltage of 200 kV), respectively.

The porous texture of the samples was characterized by N_2 adsorption-desorption at −196 °C, and by CO_2 adsorption at 0 °C performed in ASAP 2020 apparatus (Micromeritics). Samples were outgassed at 150 °C for at least 8 h. From the N_2 isotherm, the apparent surface area (A_{BET}) was determined by applying the BET equation. The t-method allows obtaining the values of the external surface area (A_t) and the micropore volume (V_t). The mesopore volume (V_{mes}) was determined following the Gurvich rule as the difference between the adsorbed volume of N_2 at a relative pressure of 0.99 (V_{tot}) and the micropore volume V_t. Dubinin-Radushkevich equation was used to calculate the apparent surface area (A_{DR}) and narrow micropore volume (V_{DR}) from

CO_2 adsorption data.

Raman spectra were recorded with a Renishaw micro-Raman system using an Ar^+ laser at 514 nm as the excitation source, with a spectral resolution of 2 cm^{-1}. The diffraction patterns of the carbon fibers were analyzed by a XRD diffractometer (Siemens D5000), over a 2θ range with Bragg–Brentano geometry using the Cu Kα radiation and a graphite monochromator. To characterize these materials, the centroid of the (002) peak was determined, obtaining the average d_{002} interlayer spacing from Bragg's equation. Additionally, lattice parameters in the parallel, L_a, and perpendicular, L_c, directions were calculated from the position and full width at half maximum (FWMH) of the (002) and (10) peaks by using the Scherrer equation. Shape factor (K) values of 0.9 and 1.84 were utilized, respectively [12].

Electrical conductivity measurements were performed on a home-made 2-probe electrochemical cell, consisting of a stainless-steel cylinder with an internal polytetrafluoroethylene (PTFE) jacket (internal diameter: 6 mm) and equipped with two titanium rods ended with PTFE stoppers as collectors. C. a. 50 mg of sample was packed between the collectors for the measurements. Afterwards, the cell was pressed up to 1 MPa by using a hydraulic press. The length of packed bed within the cell was then determined by using a micrometer (±0.05 mm). Conductivity measurements of the samples were performed while pressing in a SP-200 Biologic potentiostat working in galvanostatic mode. The bed resistance, R (ohms), is determined from the slope of the voltage vs current intensity (V–I) plot and it is later used for the determination of the electrical conductivity using the following equation:

$$\sigma = S \cdot R^{-1} \cdot L^{-1}$$

where L is the bed length (m), and S is the cross-sectional area of the cell (m^2). In all the cases, at least five V–I determinations were collected and averaged to determine the resistance of the carbon fibers.

The electrochemical behavior of CFs and PCFs in acid electrolyte (1 M H_2SO_4, Sigma-Aldrich) were evaluated using PTFE 3-electrode Swagelok cells equipped with titanium rod as current collectors. A commercial Ag/AgCl/KCl electrode was inserted through the upper connector of the cell in order to track the potential of the electrodes. The electrodes consisted in round slices (Ø: 4 mm, thickness: 0.2 mm, surface loading of 5–6 mg cm^{-2}) of the carbon fiber samples, meaning that no binder nor conductivity promoters were used in their preparation. A Nylon membrane (Milipore, Merk, mean pore size: 450 nm) was sandwiched between the carbon fiber electrodes, therefore acting as separator. Cyclic voltammetry (CV) in 3-electrode configuration was recorded between −0.2 and 0.8V vs Ag/AgCl. Reference electrode was connected to the counter electrode for operating the cell in a 2-electrode configuration. Electrochemical impedance spectroscopy (EIS) was measured at open circuit potential measurements of the electrodes. The equivalent series resistance of the cell (Rs), the charge transfer resistance (Rct) and equivalent distributed resistance (Zd) of the electrodes have been estimated from the Nyquist plots using an Randles equivalent circuit coupled with a capacitor element in Z-sim software (Bio-Logic). All measurements were carried out in a SP-200 Biologic potentiostat. Gravimetric capacitance, C_g, was obtained according with the next equation:

$$C_g = \frac{j \cdot t_d}{U - IR_{drop}}$$

where C_g is the gravimetric capacitance (F g^{-1}), j is the current density (A g^{-1}), t_d is the discharge time (s), U is the voltage (V) and IR_{drop} is the voltage drop due to cell resistance (V)

3. Results and discussion

3.1. Carbon fibers preparation and chemical composition

The morphology and size of the electrospun carbon fibers has been analyzed using scanning electron microscopy. Fig. 1 shows representative SEM micrographs of carbon fibers prepared using different H_3PO_4 mass ratios and thermal treatment temperatures, along with the evolution of the fiber diameter distribution. Each of these distributions were stablished after evaluating the diameter of more than 100 fibers. The micrographs reveal that the carbonization of the electrospun lignin solutions at 500 °C provided mats consisting in flexible, continuous and randomly-oriented fibers showing average diameter of around 2.5 μm, no matter the amount of phosphoric acid added to the solution. However, the presence of H_3PO_4 produces a larger dispersion of the sizes, as depicted by the wider fibers size distributions of the PCFL500 and PCFH500 (sizes from 0.5 to 4.5 μm for both samples, while size for CF500 ranges from 1 to 4 μm). The addition of H_3PO_4 to the solution increases the electrical conductivity, which decreases the stability of the Taylor cone produced in the electrospinning, rendering a larger variability of jet diameters and consequently, of the diameter of lignin-H_3PO_4 fibers collected on the electrospinning plate [20]. As expected, an intense shrinkage of the pure lignin fibers is observed with the increase of the preparation temperature (ca. 50% at 900 °C and of ca. 65% at 1600 °C). This shrinkage is clearly hindered by the addition of H_3PO_4 to the lignin solution, being around 45% for PCFL900, 60% for PCFL1600, and only 20% for PCFH900. Surprisingly, no shrinkage is observed in the case of PCFH1600. A likely explanation of this unexpected outcome is the existence of microporosity on this sample, Table 4, due to the presence of P in the bulk of the fibers, which has been corroborated by XPS depth profile, Fig. 3. All these features will be discussed on the next sections. In accordance to all these observed shrinkages, a narrower fiber size distribution is achieved as preparation temperature increases in these samples, exception made of PCFH1600. It must be noted that the wideness of the size distribution of P-containing fibers is always higher than that of CF at any given temperature.

Table 1 shows the mass yield of the fibers for each process step, the overall yield of the different final carbon fibers and the chemical composition by ultimate analysis. The stabilization step consists of an oxidative treatment, generating cross-links in the lignin matrix, in order to increase the glass transition temperature and prevent the fiber from fusion during carbonization step [11]. The stabilization yields increase with the amount of H_3PO_4 in the Alcell lignin solutions and vary from 87 to 76% for lignin fibers with and without H_3PO_4, respectively. The addition of H_3PO_4 results in the formation of thermally stable phosphate and/or polyphosphate esters, which generate cross-links with the lignin structure without the need to incorporate oxygen from the gas phase [20].

In general, carbonization yields decrease with temperature due to the dehydration of the precursor, the removal of the volatile matter and the possible activation of the samples. Phosphorus-containing carbon fibers present higher carbonization yields than those without phosphorus, due to the restriction of the formation of tar during the activation process, increasing the final solid weight [29]. The carbon content determined by ultimate analyses increases with the treatment temperature, meanwhile the amount of hydrogen and oxygen significantly decreases, as a consequence of devolatilization and aromatic condensation processes that are favored at higher carbonization temperatures and/or H_3PO_4 to lignin mass ratios.

High temperature thermal treatment of carbon fibers produces further increase in the carbon content and significant low oxygen content, that further decreases with temperature, particularly for the samples prepared at higher H_3PO_4/lignin mass ratio. The preparation of porous carbon materials by chemical activation with H_3PO_4 produces an increase in the oxygen surface groups due to the presence of thermally stable C–O–P and C–P–O surface groups [28,30]. The decomposition of these surface groups takes place at high temperatures (>700 °C, see TPD results in Fig. 4), explaining the lower thermal treatment yields of PCFs.

The overall yields referred to the weight of carbon fibers with respect to the initial weight of lignin are ranging from 27 to 41% for the pure carbon fibers, in agreement with those previously reported [31].

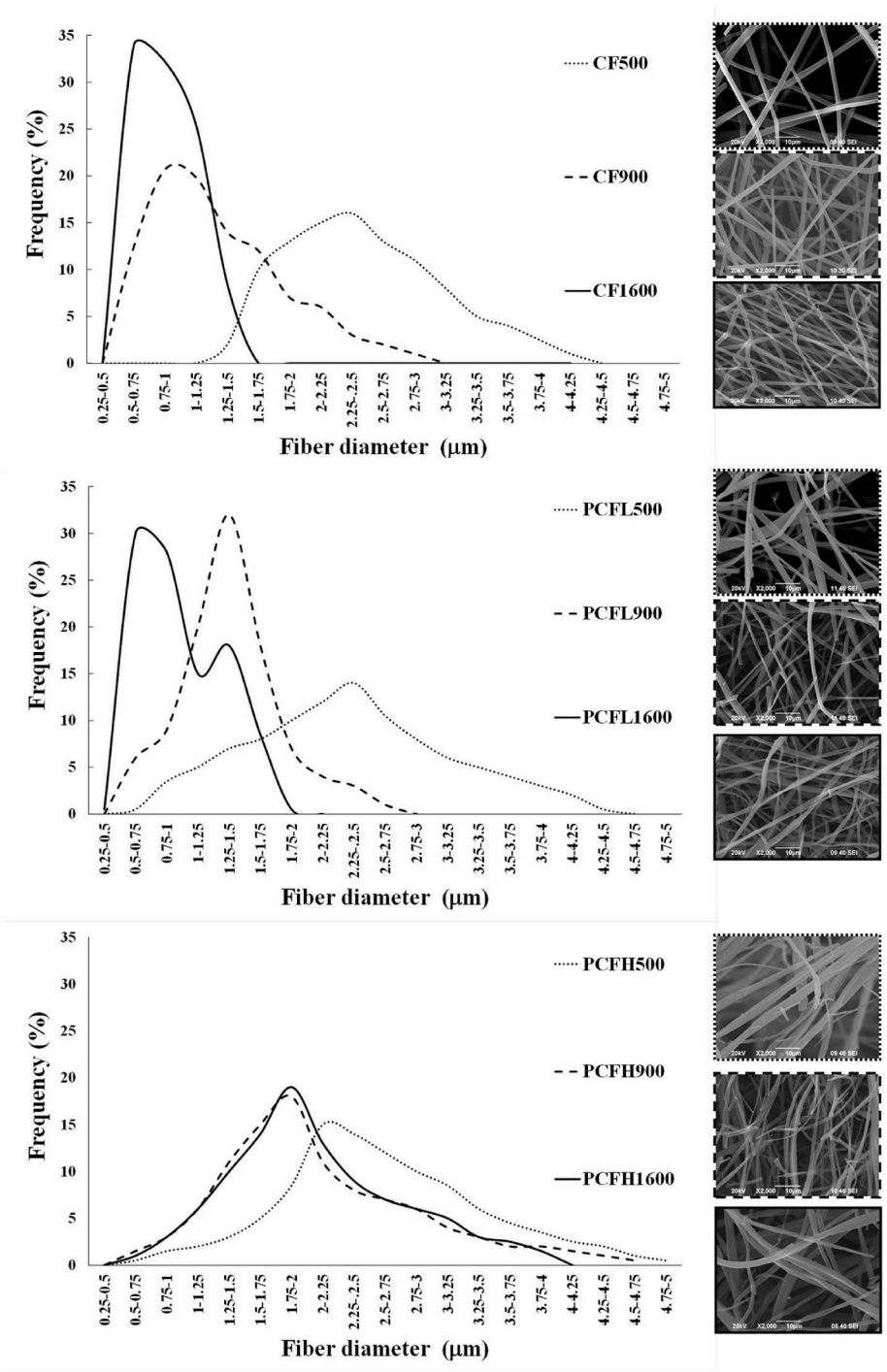

Fig. 1. Fiber diameter distribution and SEM images of CF, PCFL and PCFH carbon fibers prepared at 500, 900 and 1600 °C. Scale bar: 10 μm. (A colour version of this figure can be viewed online.)

Phosphorus-containing carbon fibers show higher overall yields at 500 and 700 °C. Those values are in agreement with those obtained by chemical activation with phosphoric acid at the same activation temperature from other biomass precursors [27,32,33]. Carbonization at 900 °C and thermal treatment at higher temperatures produces the decomposition of most of the phosphorus surface groups (Fig. 4), resulting in overall yields for PCFs similar to those shown by CFs.

3.2. Surface chemistry

Table 2 collects the C, O and P mass surface concentrations of the different carbon fibers determined by XPS and the mass concentration of phosphorus in the bulk for PCFH samples measured by ICP. In general, the surface carbon content increases and the oxygen amount decreases with the preparation temperature. In the case of CF samples, it can be associated to the higher removal of the volatile matter and to the greater release of the oxygen incorporated in the stabilization stage, in form of CO_2 and CO, during this carbonization stage [19]. For P-containing carbon fibers, the increase in the carbonization temperature and/or in the H_3PO_4 to lignin mass ratio decreases the oxygen content. The thermal treatment at high temperature provides very pure carbon fibers with oxygen content lower than 2%. As it was previously reported,

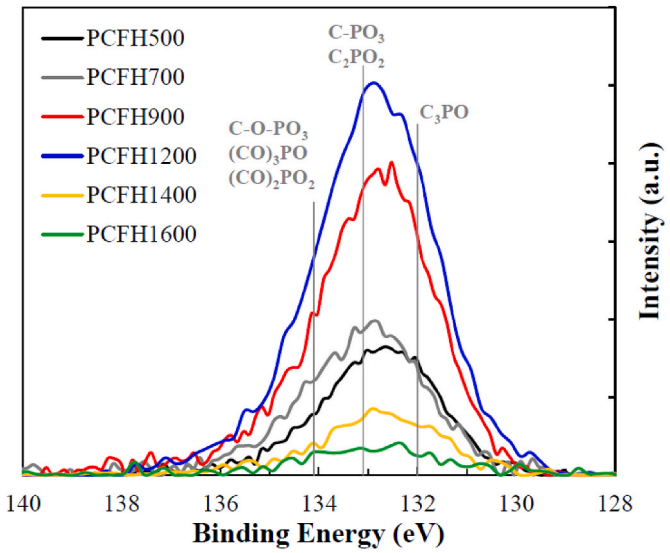

Fig. 2. XPS spectra of P 2p core-levels of phosphorus-containing lignin fibers obtained at the highest H_3PO_4 to lignin mass ratio (0.3), at different temperatures. (A colour version of this figure can be viewed online.)

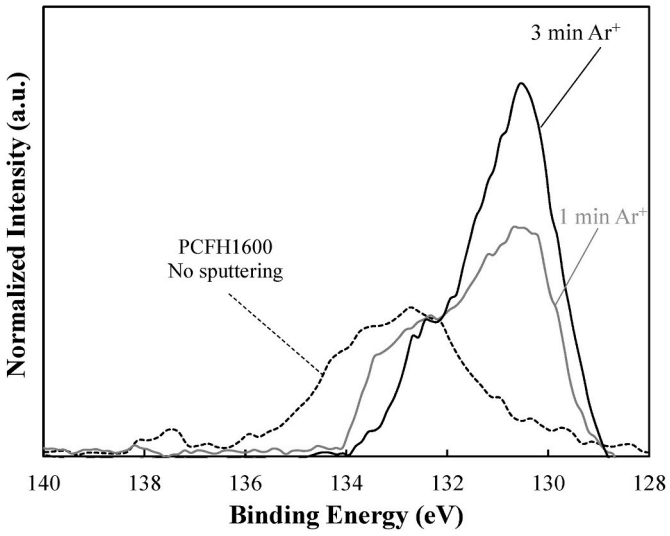

Fig. 3. P 2p region of XPS spectra from PCFH1600 at different etching times. (A colour version of this figure can be viewed online.)

phosphorus-functionalized carbon fibers present more oxygen than CFs, due to the presence of phosphorus surface groups (e.g., C-O-PO_3 like groups) [30,34]. Furthermore, some devolatilization of phosphorus compounds is also observed at 1400 °C, generating PCFs with high purity (P surface content as low as 0.3% for PCFH1600). The comparison of the phosphorus content measured by XPS and ICP suggests that the phosphorus is mainly located in the external surface of the fibers prepared at temperatures lower than 1200 °C. At higher temperatures, a decrease of the phosphorus content is probably produced by reduction and devolatilization on the most outer surface of the carbon fibers, as pointed out by the lower amount detected by XPS.

The analysis of the P 2p spectra of the PCFs was carried out in order to determine the kind of P-surface groups found on the carbon fibers. Fig. 2 shows the P 2p spectra of PCFs prepared at H_3PO_4 to lignin mass ratio of 0.3 and at different thermal treatment temperatures. The contribution of mainly three species of phosphorus are observed, which are located at i) 134.1 eV attributed to –C–O–PO_3, –$(CO)_2$–PO_2 or –$(CO)_3$–PO species; ii) 133.1 eV associated to –C–PO_3 or –C_2–PO_2 species and; iii) 132 eV assigned to phosphorus reduced –C_3–PO species. In most samples, the band centered at 133.1 eV is the most relevant, which is characteristic of C–P bonding as in C-PO_3 groups, where P is bonded to one C and three O atoms (two single and one double bonds), and/or C_2PO_2 [28]. The thermal treatment does not seem to modify the relative contribution of the different P functionalities on the PCFH900. However, PCFH samples prepared at lower temperatures (PCFH500 and PCFH700) present a slightly higher proportion of the more oxidized species. Previous results with another biomass precursor also showed that an increase in the activation temperature shifts the main peak to lower values (around 133.2 ± 0.2 eV), associated to the presence of less oxidized species [30].

In order to verify that phosphorus is located inside the carbon fibers, particularly (mostly) for those prepared at temperatures higher than 1200 °C, P 2p region of the depth-profile XPS spectra were collected in Fig. 3 after submitting PCFH1600 at two different argon sputtering times. An important shifting of the peak to lower binding energy (130.3 eV) was observed just after 1 min of argon ion sputtering, revealing the presence of less oxidized P species in the inner of the carbon fibers, probably in form of C_3– P one (and C_3–PO). Further increase on the sputtering time delivers both a higher P concentration (increasing 9.2 and 22.1% from the starting concentration after one and 3 min of sputtering time, respectively) and a larger contribution of these C_3– P species (negligible amount of C_3– P in the starting spectra vs contribution of more than 80% of this P species after sputtering for 3 min), confirming that phosphorus concentration increases in the core of the PCFH1600 carbon fibers, being preferentially in form of less oxidized species.

Fig. 4 collects CO and CO_2 evolution during TPD experiments of the three series of carbon fibers. As can be seen, the amount of CO-evolving groups in all samples is significantly higher than that of oxygen surface groups decomposing as CO_2. Overall, the presence of oxygen containing functionalities decreases with the preparation temperature, especially in the case of CF samples. In addition, the evolution of CO and CO_2 for CF series is much lower than that found in PCFs series, at all temperatures, with the exception of the sample carbonized at 500 °C. According to XPS data, the oxygen surface concentration of CF500 is quite high (15.4% O), as a consequence of the presence of volatile matter and oxygen incorporated in the stabilization stage, which have not been released during carbonization. In this line, results previously reported [17] showed a broad CO evolution curve up to high temperatures (>700 °C), related to the thermal release of anhydride, phenol, ether and/or carbonyl groups as a consequence of char formation reactions, which suggests that these reactions are not completed at 500 °C and are probably taking place during the TPD analysis of CF500.

The addition of phosphoric acid to the lignin solution produces a decrease of CO and CO_2 released at temperatures lower than 700 °C, as observed for PCFL500 and PCFH500, pointing out the presence of a lower amount of anhydrides and phenolic groups. This decrease is probably related to the dehydration and crosslinking reactions taking place between phosphoric acid and hydroxyls/phenolic functionalities during the air stabilization stage. An increase in the CO evolved at high temperatures (700–900 °C) due to the decomposition of phosphorus functional groups is also observed in these samples. Rising the carbonization temperature from 500 to 900 °C produces a shift of the whole curve to higher temperatures. PCFH900 and PCFL900 samples show the maximum CO desorption rate at 860 °C, assigned to the decomposition of stable C–O–P surface groups, producing CO and C′-P surface groups, where C′ refers to a new surface carbon atom [28,30].

As for the samples treated at 1200–1600 °C, it is worthy to mention the relatively high CO evolution of samples PCFL1200 and PCFH1200 when compared to that of CF1200. The CO evolution of the former samples again peaked at 860 °C, indicating the presence of C–O–P type groups. We have reported that C–P groups formed during thermal annealing at high temperatures of P-containing carbon materials can be easily reoxidized upon contact with air, forming again the C–O–P type

Table 1
Ultimate analysis and preparation yields of carbon fibers.

Carbon fiber	Yields (%)				Ultimate analysis		
	Stabilization	Carbonization	Thermal treatment	Overall	C (%)	H (%)	O[a] (%)
CF500	76.0	54.5		41.4	74.4	2.2	23.4
CF700		45.0		34.2	89.0	1.5	9.5
CF900		35.0		26.6	92.0	1.7	6.3
CF1200		*35.0*[b]	99.2	26.4	95.8	0.1	4.1
CF1400		*35.0* [b]	96.4	25.6	97.3	0.2	2.5
CF1600		*35.0*[b]	93.1	24.8	98.5	0.1	1.4
PCFL500	86.1	68.3		58.8	73.5	2.0	24.5
PCFL700		59.1		50.9	74.1	1.2	24.7
PCFL900		34.3		29.5	78.8	1.3	19.9
PCFL1200		*34.3*[b]	98.6	29.1	85.0	0.2	14.8
PCFL1400		*34.3*[b]	91.2	26.9	96.3	0.1	3.6
PCFL1600		*34.3*[b]	87.8	25.9	96.6	0.0	3.4
PCFH500	87.3	70.6		61.6	76.6	2.4	20.9
PCFH700		52.1		45.5	79.5	2.1	18.4
PCFH900		33.1		28.9	81.4	1.5	17.2
PCFH1200		*33.1* [b]	94.2	27.2	85.2	0.4	14.3
PCFH1400		*33.1* [b]	87.2	25.2	94.5	0.5	5.0
PCFH1600		*33.1* [b]	83.3	24.1	97.2	0.0	2.8

[a] *Calculated by difference.*
[b] *Yield of samples carbonized at 900 °C, which are the starting material in the further high temperature thermal treatment.*

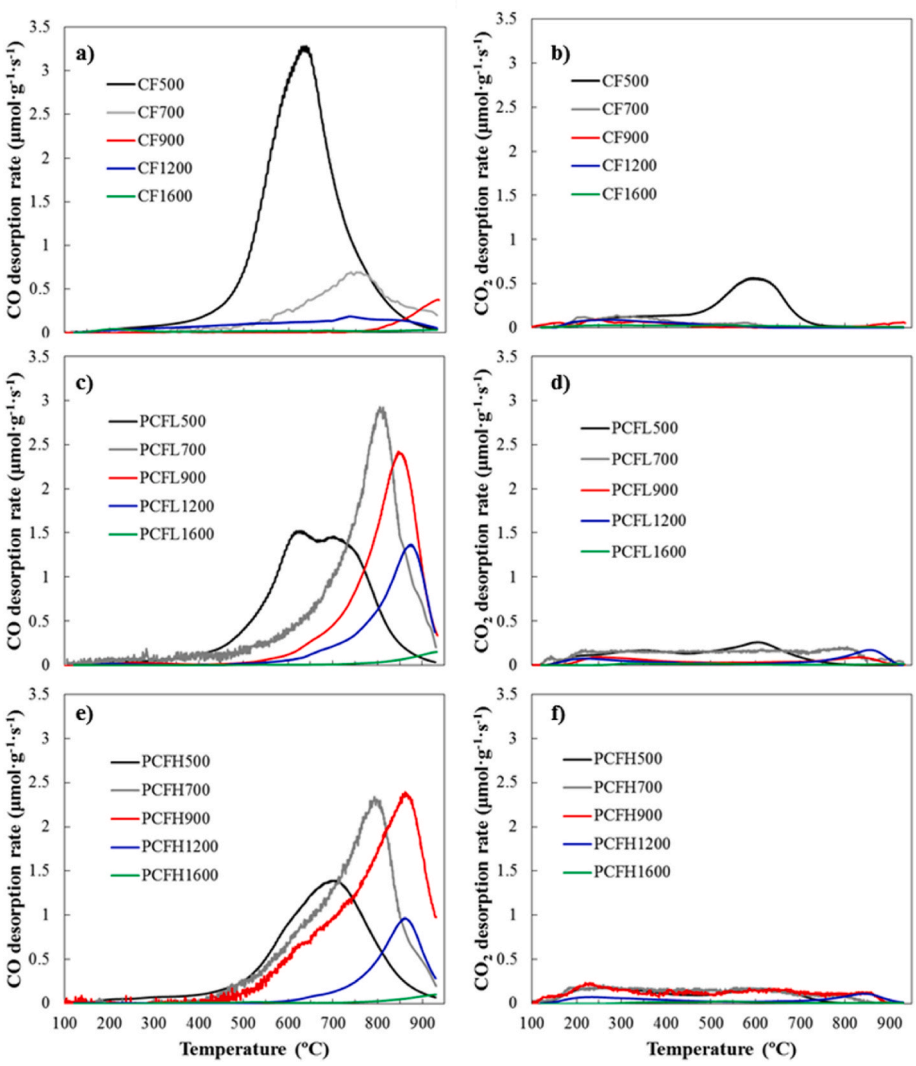

Fig. 4. CO and CO_2 evolution during TPD experiments of the three series of carbon fibers: (a), (b) CF; (c), (d) PCFL and (e), (f) PCFH, respectively, at different thermal treatment temperatures. (A colour version of this figure can be viewed online.)

Table 2
Mas surface concentration (%) determined by XPS of the carbon fibers and total phosphorus concentration of PCFH samples determined by ICP.

Carbon fibers	C_{XPS} (wt%)	O_{XPS} (wt%)	P_{XPS} (wt%)	P_{ICP} (wt%)
CF500	84.6	15.4	0.0	n.m.
CF700	92.4	7.6	0.0	n.m.
CF900	95.9	4.1	0.0	n.m.
CF1200	97.8	2.2	0.0	n.m.
CF1400	98.9	1.1	0.0	n.m.
CF1600	98.2	1.8	0.0	n.m.
PCFL500	79.7	18.2	2.1	n.m.
PCFL700	82.7	15.0	2.3	n.m.
PCFL900	83.2	14.2	2.6	n.m.
PCFL1200	91.8	5.4	2.8	n.m.
PCFL1400	97.0	2.5	0.5	n.m.
PCFL1600	97.3	2.1	0.6	n.m.
PCFH500	85.8	13.2	1.0	0.7
PCFH700	87.2	11.1	1.3	1.0
PCFH900	90.2	7.4	2.4	1.3
PCFH1200	90.3	6.6	3.1	2.3
PCFH1400	98.0	1.5	0.5	1.5
PCFH1600	97.9	1.8	0.3	0.7

n.m.: not measured.

groups [28]. This phenomenon is not observed in the samples treated at 1600 °C due to the loss of most of the surface phosphorus groups (see P contents by XPS in Table 2), producing a low evolution of CO and CO_2, as observed for PCFL1600 and PCFH1600, still slightly higher than that of CF.

3.3. Structural order characterization

Changes on structural order generated by thermal treatment of carbonized lignin under inert atmosphere were studied by Raman and X-ray diffraction spectroscopy, demonstrating that highly ordered carbon materials can be obtained from lignin [12]. Fig. 5 compares the first-order Raman spectra of the three series of carbon fibers prepared in this work in order to follow changes in structural order due to the presence of phosphorus and the increase in the preparation temperature. All curves present characteristic features of carbon materials, i.e. presence of two broad Raman bands at ca. 1350 cm^{-1} (presence of disordered carbon, D band) and 1590 cm^{-1} (graphitic-like structure, G band) that get narrower and more intense with temperature [35,36]. In addition, the development and narrowing of the bands at 2700 cm^{-1} (2D band) and 2940 cm^{-1} (D + G band) line of the second order spectra (inset in Fig. 5) with the carbonization/high temperature treatment are also noticed, confirming the advance of the structural order with temperature [37–39].

Fig. 5. d provides a direct comparison between the Raman spectra of the carbon fibers obtained at 1600 °C. Similar spectra are recorded for the three samples, with the narrower D band belonging to PCFH1600, which also shows the clearer development of the 2D and D + G bands in the second-order spectra region. Lateral size of the crystallites (L_a) on these samples has been determined using the formula stablished by Knight and White (L_a=*4.4*·I_G/I_D, nm [40]), showing values of 4.6, 4.9 and 4.5 nm for CF1600, PCFL1600 and PCFH1600, respectively. These results seem to point out that the presence of phosphorus does not significantly modify the development of this lattice parameter of carbon fibers.

Deconvolution of Raman spectra into four bands was used to obtain some further information about the structural order, in accordance to our previous studies about electrospun lignin-based carbon fibers [17]. The deconvolution includes the D and G lines and two additional bands at 1170 cm^{-1} and 1510 cm^{-1} that are attributed to the presence of oxygen groups and other heteroatoms and interstitial defects, respectively [41,42]. Table 3 summarizes a selection of the obtained deconvolution parameters. Again, the presence of phosphorus seems to have a low effect in the structural order of the carbonized fibers determined by Raman. In all the series, the integrated I_G/I_T ratios (i.e. ratio between the integrated intensity of G peak and the integrated intensity of all the deconvoluted peaks) show a small development of G peak at 1600 °C and a clear narrowing of the width of the D line with the preparation temperature. Both features are regarded as an evidence of structural ordering development [36,37,41]. Lastly, the I_{1170}/I_T ratio, which is

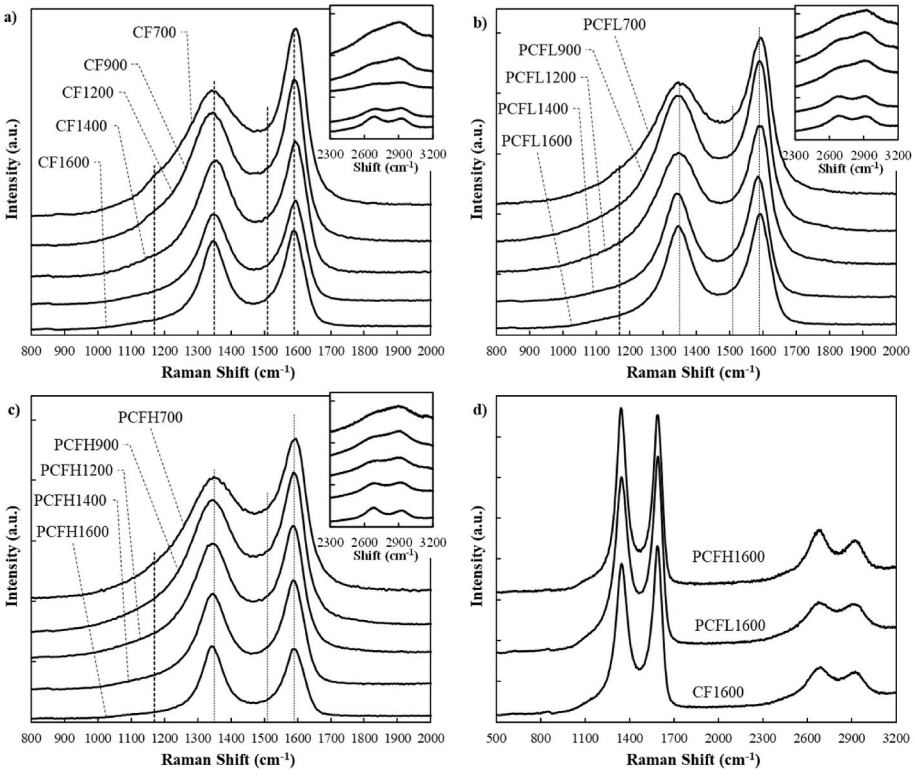

Fig. 5. First-order region of the Raman spectra of the three series of lignin-fibers carbonized at different temperatures. a) CF series b) PCFL series; c) PCFH series. Dotted line guides at 1170, 1350, 1510 and 1590 cm^{-1} are plotted for indicating the position of the main bands used in the deconvolution of the Raman spectra. Inset shows the respective second-order Raman spectra region. d) Comparison of full Raman spectra from pure and P-containing lignin fibers prepared at 1600 °C. (A colour version of this figure can be viewed online.)

Table 3
Selected first-order Raman spectra deconvolution parameters.

Temperature	Integrated I_G/I_T (%)			$FWMH_D$ (cm^{-1})			Integrated I_{1170}/I_T (%)		
	CF	PCFL	PCFH	CF	PCFL	PCFH	CF	PCFL	PCFH
700	26.6	25.7	25.6	198	206	224	2.6	1.8	1.9
900	25.0	23.3	22.7	180	172	181	2.5	1.9	1.9
1200	26.6	26.4	22.4	147	134	153	2.6	2.7	2.1
1400	27.2	27.3	26.5	120	119	116	1.8	2.8	4.9
1600	29.4	27.4	31.4	104	115	89	1.6	2.1	4.2

related to the presence of heteroatoms, decreases after the heat treatments at 1400 and 1600 °C of sample CF900. However, this ratio is higher for the heat-treated PCFL and PFCH samples, confirming the presence of phosphorus even after the thermal treatment at the highest temperatures, as pointed out by XPS (Table 2).

X-ray diffraction profiles have also been used to follow the structural order of lignin-based carbon materials [12]. In general, the profiles confirm that carbonized samples have a low structural order, which starts to develop after the high temperature heat treatment. For a better understanding of the effect of the presence of phosphorus on the structural lattice parameters, a direct comparison of the XRD profiles of PCFH1600 and CF1600 samples is shown in Fig. S1 of the electronic supporting information (ESI). Large X-ray scattering at small angles is observed in them due to the presence of well-developed narrow microporous structure (see CO_2 pore volumes in Table 4). The intensity of this scattering is higher in P-containing carbon fibers, in agreement with the larger narrow micropore volume observed for PCFH1600. This sample also shows a greater width of the (002) peak, which can be associated to a lower thickness of the crystal in perpendicular direction to the graphite-like layers (L_c) for this sample. In addition, no significant difference is observed in the shape of the (*10*) peaks, i.e. the one related to the size of the crystal in the parallel direction of the graphite-like layers, L_a.

The deconvolution of the (*002*) peak allows to deepen in the study of the structural order of these samples, revealing that the d_{002} interlayer spacing is 3.8 Å and 4.0 Å for CF1600 and PCFH1600, respectively. These values are in agreement to those reported for high-temperature carbons prepared from lignin at a similar temperature range [12]. The average thickness of the crystallite is also higher in the pure lignin fibers (8.7 Å for CF1600 vs 7.6 Å for PCFH1600), with a 17% decrease of the average number of graphitic planes (estimated as L_c/d_{002}) being measured for PCFH1600. The deconvolution of the (*10*) peaks confirms the Raman findings about the average lateral size of the crystallites being unaffected by the presence of phosphorus (L_a of 4.0 nm for CF1600 vs 4.1 nm for PCFH1600). It seems that, although phosphorus can delay the stacking of the basic structural units of the carbon fiber, it does not affect the edge-to-edge association between crystallites that are responsible of lateral growth of the graphene layers.

In view of the above results, the carbon fibers treated at high temperatures were analyzed by means of TEM (Fig. 6). The microstructure of P-free and P-containing carbon fibers cannot be distinguished when the heat treatment is performed at 1200 °C, Fig. 6 a and c. The images depict the expected disordered structure of porous activated carbon fibers [43]. However, the presence of phosphorus seems to produce differences in the carbonaceous matrix microstructure with a further increase of the heat treatment temperature. For the carbon fibers treated at 1600 °C in the absence of phosphorus (CF1600), the structure is dominated by long and straight graphitic planes, which runs parallel to the surface of the carbon fiber (see Fig. 6d). Differently, the presence of phosphorus renders the formation of long, curved and strained graphene layers, as those seen in TEM image of PCFH1600 (Fig. 6b), confirming that the presence of phosphorus hinders the stacking of carbon microcrystallites. Theoretical studies on the bonding of atomic P to graphene systems based on Density Functional Theory have shown a marked tendency for P-induced inter-linking of the graphene that breaks the continuity of the planes and that the bonding of P atoms both induces and enhances strong local curvature in such graphitic structures [44,45]. In this sense, a theoretical study on the bonding of atomic phosphorus to planar hydrocarbons and to curved graphite-like surfaces concluded that bonding phosphorus to planar polycyclic hydrocarbons induces curvature away from the phosphorus atom and that the ability of the carbon atoms of these systems to maintain or induce curvature is a prerequisite condition for stably bonding of atomic phosphorus [46]. The origin of this curvature can rely on the generation of a charge transfer between the phosphorus and the carbons, creating new charge concentrations that make curved geometry energetically favorable [46]. Experimental

Table 4
Textural properties derived from the N_2 adsorption–desorption isotherms and CO_2 isotherms at −196 °C and 0 °C, respectively, of the three series of carbon fibers at the different thermal treatment temperatures.

Carbon fibers	N_2 Isotherm					CO_2 Isotherm	
	A_{BET} m^2g^{-1}	A_t m^2g^{-1}	V_t cm^3g^{-1}	V_{mes} cm^3g^{-1}	V_{tot} m^3g^{-1}	A_{DR} m^2g^{-1}	V_{DR} cm^3g^{-1}
CF500	326	11	0.122	0.015	0.137	505	0.203
CF700	413	16	0.159	0.018	0.177	652	0.261
CF900	840	7	0.329	0.008	0.337	951	0.381
CF1200	621	5	0.239	0.007	0.246	749	0.300
CF1400	530	13	0.204	0.017	0.221	669	0.268
CF1600	20	16	0.003	0.021	0.024	253	0.101
PCFL500	398	16	0.153	0.018	0.171	508	0.204
PCFL700	556	11	0.215	0.014	0.229	630	0.252
PCFL900	951	5	0.366	0.007	0.376	798	0.320
PCFL1200	758	11	0.300	0.014	0.314	751	0.301
PCFL1400	719	11	0.277	0.014	0.291	698	0.280
PCFL1600	646	13	0.252	0.016	0.268	609	0.244
PCFH500	749	14	0.294	0.015	0.309	803	0.322
PCFH700	837	10	0.326	0.012	0.338	842	0.338
PCFH900	1143	16	0.449	0.017	0.466	859	0.344
PCFH1200	921	13	0.361	0.014	0.375	803	0.322
PCFH1400	908	11	0.368	0.012	0.380	739	0.296
PCFH1600	822	15	0.327	0.017	0.344	599	0.240

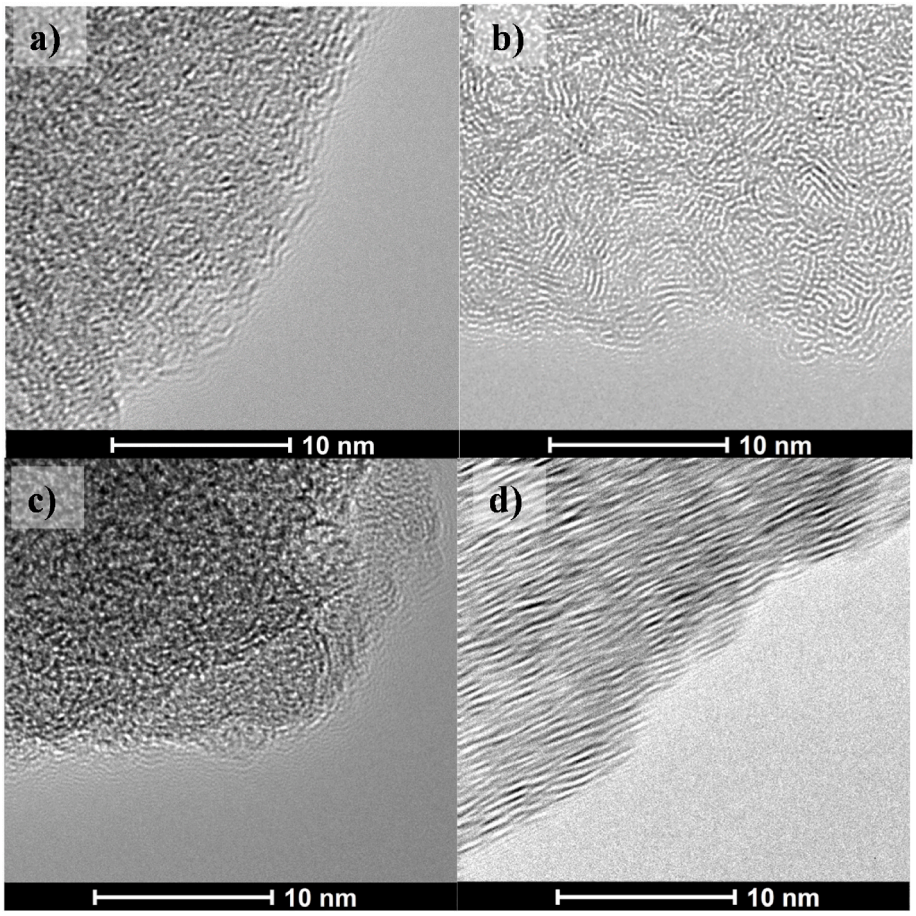

Fig. 6. TEM images of a) PCFH1200 b) PCFH1600, c) CF1200 d) CF1600. (A colour version of this figure can be viewed online.)

results on phosphorus carbides thin films corroborated these results and indicated that the induced graphene layer curvature increases the inter-layer distances [47,48].

3.4. Textural properties

With regard to the influence of the presence of P on the porosity of the lignin-derived carbon fibers, Fig. 7 shows the N_2 adsorption–desorption isotherms at −196 °C of the pure carbon fibers and phosphorus-containing carbon fibers obtained at different preparation temperatures. Textural parameters derived from N_2 (−196 °C) and CO_2 (0 °C) adsorption data for the different carbon fibers are summarized in Table 4. All the fibers exhibit a type I isotherm, characteristic of microporous solids. Previous studies revealed that the high oxygen content in the stabilized Alcell fibers could also act as activating agent during carbonization step, producing a decrease of the carbonization yield as a consequence of a development of microporosity [11,17]. At the same carbonization temperature, higher N_2 adsorbed volumes (at very low relative pressures) were observed as the H_3PO_4/lignin mass ratio increases, showing increasing A_{BET} values from 326 $m^2\ g^{-1}$ for CF to 749 $m^2\ g^{-1}$ for PCFH, at 500 °C. The high values of the micropore volume measured with CO_2 (compared with those of N_2) indicate the presence of narrow microporosity. The presence of mesoporosity is quite low in all samples (V_{mes} lower than 0.02 $cm^3\ g^{-1}$). An increase of the H_3PO_4/lignin mass ratio above 1 would provide the development of wide mesopores, as we have observed with other lignocellulosic precursors [30,49]. However, the use of higher amounts of phosphoric acid provides solution with greater conductivity values, hindering the spinnability of the solution.

In general, the maximum development of porosity is obtained in samples carbonized at 900 °C, independently of the presence of phosphorus. The micropore volume and surface area of the P-free lignin-derived carbon fibers slightly decrease after thermal treatments at temperatures between 1200 and 1400 °C. However, an accused decrease of the porosity is observed when the treatment temperature was increased above 1400 °C for carbon fibers that did not contain phosphorus. In this sense, it is important to highlight the differences among the N_2 isotherms of PCFL1600 and those of PCFH1600 and CF1600. Very low nitrogen adsorption at −196 °C is measured for the latter sample, pointing out the reduction of most of the porosity ($A_{BET} = 20\ m^2 g^{-1}$) with the high temperature treatment. A similar porosity shrinkage is observed for activated carbon fibers with A_{BET} comparable to that of CF900 when they are heat treated at 1500 °C [50]. However, PCFL1600 and particularly PCFH1600 show a large N_2 uptake, which translates into an apparent surface area of 820 $m^2\ g^{-1}$ in the case of the latter sample, despite the high treatment temperature used. Given the similar structural order and surface area of both CF900 and PCFH900 samples, the presence of phosphorus seems to be responsible of the low porosity shrinkage observed for the last one with increasing temperature. In this sense, TEM images of PCFH1600 in Fig. 6 evidenced that the presence of phosphorus prevents from the staking of carbon microcrystallites that takes place in the case of CF1600, which could be the reason of the porosity preservation shown by PCFH1600. Thus, the voids between the microcrystallites, which correlates with microporosity, are larger in PCFH1600 because the hindered stacking of their curved graphene layers. The results of XPS, TPD, Raman, TEM and N_2/CO_2 adsorption isotherms allow concluding that structural order is not severely compromised neither by the presence of phosphorus nor by a more developed pore structure in PCFH1600 (with A_{BET} >820 $m^2\ g^{-1}$). This combination of desirable features is usually hard to achieve. For

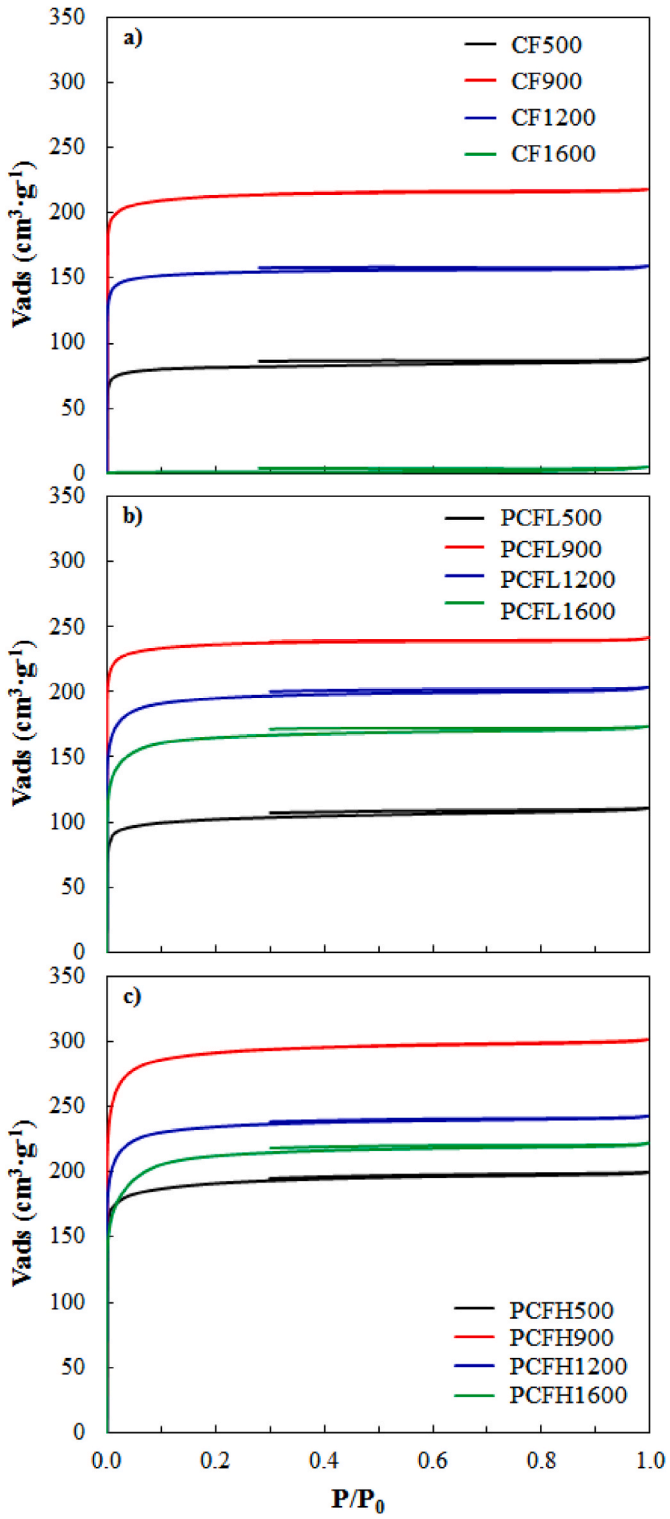

Fig. 7. N_2 adsorption–desorption isotherms at −196 °C of the three series of carbon fibers: (a) CF; (b) PCFL and (c) PCFH series, respectively, at the different carbonization temperatures. (A colour version of this figure can be viewed online.)

instance, the shape and intensity of D and G bands for other porous lignin-based carbon fibers clearly shows the loss of structural order when the carbonized fibers are submitted to a chemical activation method [51]. Thus, the carbonization of phosphorus-functionalized lignin fibers followed by high temperature heat treatment can overcome the degradation of structural order. In this regard, some authors have reported the thermal treatment at 1500 °C of electrospun lignin-derived carbon fibers using polyvinyl alcohol as a binder. These fibers showed A_{BET} of 940 $m^2\ g^{-1}$, but also presented a very high oxygen content (12.1%, determined by ultimate analysis), which suggests that a slight gasification was taken place [52]. Furthermore, neither the mass yield for the preparation of the carbon fibers nor their structural order were reported.

3.5. Electrical conductivity

In view of an adequate combination of chemical composition, morphology, microstructure and porosity, the lignin-derived carbon fibers presented in this work could have potential electrochemical and photovoltaic applications [53–55]. In fact, carbonized lignin was recently proposed as a potential alternative to carbon blacks [56], even though the electrical conductivity achieved at carbonization temperature of 900 °C is not enough to match that of commercial carbon blacks. The electrical conductivity of the prepared carbon fibers, a decisive factor for these applications, was determined at different carbonization and heat treatment temperatures by using a 2-probe method (Table 5). At low preparation temperatures, pure lignin-based carbon fibers present lower electrical conductivity than those prepared with phosphoric acid in their formulation. As previously mentioned, phosphoric acid catalyzes dehydration and condensation reactions, as pointed out by the carbon contents in Table 1. Aromatization of the carbon structure is one of the requisites for enabling electrical conductivity of carbon materials, explaining why the addition of H_3PO_4 improves the electrical conductivity at low and mild carbonization temperatures. At 900 °C, polycondensation and dehydrogenation reactions take part in the carbonization of pure carbon fibers, enabling the formation of polycyclic aromatic structures that increases the electrical conductivity [57]. In addition, phosphates and polyphosphates (see P content on Table 2) at edge positions of these structures are believed to behave as electron-withdrawing groups, decreasing the conductivity of PCFH when carbonized at 900 °C [58]. The conductivity values shown by the carbon fibers obtained at 900 °C, either with or without H_3PO_4 in their formulation, are comparable to other electrically conductive carbon materials, such as activated carbons [59], glassy carbons [60], carbon blacks [61] and petroleum pitch based activated carbon fibers [62]. They are higher than those reported for carbonized lignin powder at 900 °C, around 1 S m^{-1} [56], or electrospun carbon fibers prepared at 1000 °C from blends of kraft lignin and PEO, 231 S m^{-1} [63] and only lower than the value obtained for graphene grafted carbon nanofibers prepared at 1100 °C by electrospun of calcium lignin sulfonate, 2378 S m^{-1} [64].

As for the effect of the heat treatment at higher temperatures, conductivity clearly increases with temperature, obtaining a linear relation for the electrical conductivity and the preparation temperature (see Fig. S2) at preparation temperature from 900 °C. In the case of PCFs, similar slopes were found, being of 0.85 and 0.81 S m^{-1} $°C^{-1}$ for carbon fibers prepared at low and high H_3PO_4/lignin mass ratio, respectively. On the other hand, for CFs, a high value of this slope, of 1.42 S m^{-1} $°C^{-1}$, is obtained. Electrical conductivity increases between 2 and 2.5 times at 1600 °C for all the carbonized fibers. Similar improvement upon electrical conductivity was reported for glassy carbon, which was found to

Table 5
Electrical conductivity of carbonized and heat-treated fibers, (S m^{-1}).

Temperature (°C)	CF	PCFL	PCFH
500	10^{-6}	$6{\cdot}10^{-4}$	7
700	1	70	115
900	670	630	450
1200	1046	919	756
1400	1402	1058	894
1600	1640	1230	1020

double the value of electrical conductivity at room temperature after heat treatment at 1600 °C [60]. The achieved values are comparable to those of composite electrodes of carbon black and chemically activated electrospun carbon fibers of surface areas ca. 1300 m^2g^{-1}, ca. 1500 S m^{-1} [65], or lignin-based porous carbon monoliths (S_{BET} of 800 m^2g^{-1}) obtained through templating methods, 1700 S m^{-1} [66], but without requesting the use of conductivity promoters, templating agents or activation treatments. It is important to note that the presence of P in the carbon fibers does not yield a notable drop of conductivity, while the preservation of microporosity on these samples constitutes a highly valuable feature of these materials. In fact, the differences in conductivity of samples prepared at 1600 °C mostly arises from their porosity. When bulk density is considered for the estimation of the conductivity of solid fiber, the value for CF1600 is only 8% and 11% higher than that of PCFL and PCFH samples (4285 vs 3980 and 3870 S m^{-1} of solid fiber, respectively). Other relevant properties, such as flexibility or mechanical strength, have been previously reported for similar lignin-based carbonized fibers at 900 °C [20,67]. A comparable flexibility has been observed for the materials reported on this work.

3.6. Electrochemical characterization

The production of continuous mats by carbonization of electrospun fibers allow preparing binderless electrodes that are known to have enhanced performance as electrodes of fuel cells and supercapacitors [18,19,21,68]. We have analyzed the potential application of the carbon fibers reported in this work for the latter application by measuring the steady state cyclic voltammetry of CF, PCFL and PCFH series in acid electrolyte (1 M H_2SO_4), shown in Fig. 8. It is important to note that these materials have been directly used as electrodes, avoiding additional preparation steps or the use of binders or conductivity promoters. It can be seen that square-box CVs characteristic of a capacitive material are observed for most of the samples. Nevertheless, the preparation temperature has different effect in the electrochemical response of CF and PCFL/PCFH series.

In the case of CF samples, the low electrical conductivity of CF700 (Table 5) is translated into a resistive response of the electrode (gravimetric capacitance ~1 F g^{-1}). In accordance to our previous works, it is found that carbonization at 900 °C produces a capacitive response of the electrode, due to the increase in the electrical conductivity and the presence of well-developed microporosity [21]. It is also worth noting the contribution of highly reversible redox process at ca. 0.35 V, which is related to the presence of electroactive functional groups, such as the quinone/hydroquinone pair [69,70]. However, the thermal treated sample CF1200 shows a capacitance decrease and slightly titled CVs in the positive potential region (around 0.7–0.8 V, Fig. 8a) despite its improved electrical conductivity (Table 5). The latter finding is probably connected to the diffusional constraints found at positive polarization by sulphate anions when moving in the narrow porosity of the sample, usually named ion sieving effect [71]. Gravimetric capacitance peaked at 900 °C in these samples, showing values of 1, 134 and 99 F g^{-1} for CF700, CF900 and CF1200, respectively. These values are within the range reported for carbon fiber electrodes with similar microporosity development [20,21,67] and in accordance with the expression developed by Lobato et al. for relating capacitance and porosity for carbon electrodes [72]. In this sense, the positive effect of microporosity on the gravimetric capacitance of electrospun carbon fibers has already been reported in the literature [21]. Expanding micropore volume from 0.33 up to 0.97 cm^{-3} g^{-1} increases the gravimetric capacitance from 130 up to 240 F g^{-1}. However, other performance parameters show different trends. Surface capacitance (Cg A_{BET}^{-1}) is not improved by activation and volumetric capacitance reaches a maximum value at micropore volumes ca. 0.50 cm^{-3} g^{-1}.

Even though microporosity is the main variable for increasing capacitance, the wettability of micropores by the electrolyte is also necessary for the development of the electrical double layer [73]. Thus,

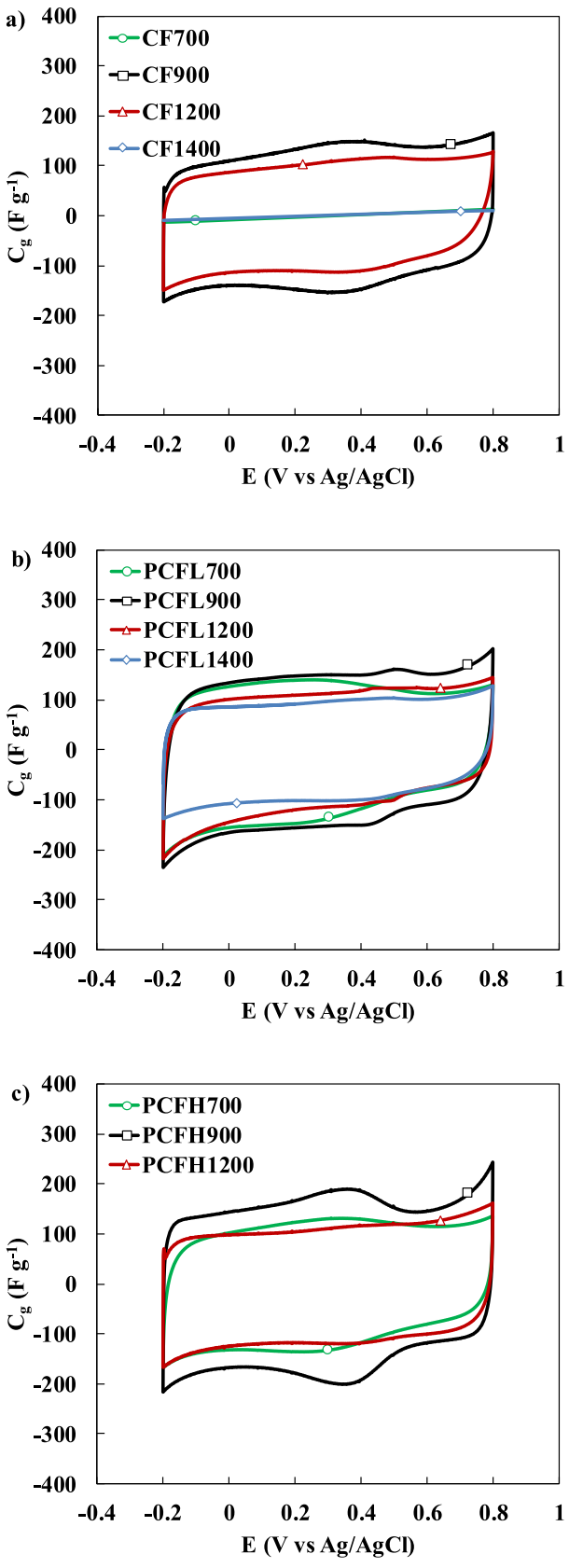

Fig. 8. Steady state cyclic voltammetry of a) CF, b) PCFL and c) PCFH series. Electrolyte: 1 M H_2SO_4. Scan rate: 10 mV s^{-1}.

further increase of heat treatment temperature delivered a total resistive behavior of the electrodes due to high hydrophobicity of the samples, which is in agreement with the loss of most of the oxygen functional groups at 1200 °C, Fig. 4. Removal of these functional groups decreases the wettability of the inner surface of the pores and therefore reduces the accessible surface area available for the electrolyte and the formation of the electrical double layer [74].

Interestingly, the PCFL series show a different pattern for the dependence of electrochemical response with temperature, especially at 700 and 1400 °C. Thus, PCFL700 shows a capacitive behavior, as expected from its higher electrical conductivity, Table 5. A small pseudocapacitive contribution related to the electroactive oxygen groups at ca. 0.45 V is also detected for PCFL900. In contrast with the loss of capacitive behavior shown by CF1400, PCFL1400 features a box-shaped CV, Fig. 8b. XPS and ICP analyses revealed the presence of oxidized phosphorus groups in this sample, Table 3, which probably enhances the surface polarity, increasing the surface area available to ions in this sample [74]. In addition, the gravimetric capacitances of PCFL700, PCFL900 and PCFL1200 are higher than their P-free counterparts, being 121, 141 and 112 F g^{-1}, respectively. Similar conclusions arise from the CVs recorded on PCFH700, PCFH900 and PCFH1200 samples, Fig. 8c, showing C_g values of 111, 175 and 112 F g^{-1}, respectively. These values are higher than those obtained for polyacrylonitrile (PAN)/pitch/lignin-based carbon nanofibers (CNFs) with ZnO [75], and comparable to those reported for hardwood and softwood lignin-based carbon nanofibers, although in alkaline electrolyte [76]. The superior capacitance of P-containing fibers no longer holds when the contribution of their higher surface area is discounted by normalizing the capacitance using A_{BET} values (surface capacitances of 0.22, 0.15 and 0.15 F m^{-2} for PCFL700, PCFL900 and PCFL1200; 0.13, 0.15 and 0.12 F m^{-2} for PCFH700, PCFH900 and PCFH1200; and 0.15 F m^{-2} for both CF900 and CF1200, respectively). A possible explanation of the higher surface capacitance of PCFL700 could be the pore size. In this sense Chmiola et al. proposed that narrow micropores could enhance the capacitance in aqueous electrolyte [77,78]. However, PCFL700 have a V_t/V_{DR}^{CO2} ratio similar to CF900 and larger than CF1200, which speaks about the mean micropore size being similar or slightly larger in the P-containing sample [79]. Therefore, the large amount of oxygen and phosphorus groups in PCFL700 (Table 2) probably increases capacitance through additional pseudocapacitance contribution from electroactive surface groups [80], which could be related to the presence of broader redox peak at potentials from −0.2 to 0.3 V in the CV [81]. In accordance with this hypothesis, the redox peaks decrease progressively with the preparation temperature due to the decomposition of electroactive hydroxyls, carbonyls and quinones groups during the carbonization and after the thermal treatments (which can be observed in the changes of CO TPD profiles in Fig. 4), losing their pseudocapacitive contribution. This is especially noted by the disappearance of all redox contribution in PCFL1400, Fig. 8b. Another desirable electrochemical feature of P-containing carbon materials is a higher electrochemical stability, meaning that the potential window for electrochemical water decomposition is widened [82]. Previous studies have also demonstrated that phosphorus groups avoid the electrochemical oxidation of carbon materials owing to the higher oxidation potential of C–O–P groups [83]. These advantages have allowed to prepare supercapacitors with P-containing electrospun carbon fibers that operates at voltages as high as 1.5 V [21], boosting the energy density of the device.

The power capability is the most important feature of supercapacitors [84]. Electrode materials for this application need to retain most of their capacitance values when submitted to high and variable power demands. Thus, the rate performance of PCFL series have been analyzed measuring the capacitance using a symmetrical 2-electrode cell configuration in the same electrolyte and operating in a 1.2 V window at increasing current density from 0.5 to 68 A g^{-1}, Fig. 9a. Gravimetric capacitance is reported in terms of electrode capacitance (4 x cell capacitance). CF1200 and PCFH1200 have been also included for comparison purpose. It can be seen that gravimetric capacitance declines with the current density, although the slope of the decrease varies between samples. An improvement of the capacitance retention (ratio of capacitances determined at scan rates of 0.5 and 68 A g^{-1}) is observed with preparation temperature, moving from a value of only 3.3% of PCFL700 to 41, 63 and 58% for PCFL900, PCFL1200 and PCFL1400, respectively. The capacitance retentions of CF1200 and PCFH1200 are 69% and 50%, showing a clear relationship with the electrical conductivity values reported on Table 5. The capacitance retention values of ca. 70% are between the highest obtained by electrospun carbonized fibers, in some cases surpassing the values obtained by more complex preparation procedures, as step-by-step electrospinning, boron and nitrogen doping [85–89].

The improvement on capacitance retention with temperature in the PCFL series seems to be related to the electrical conductivity, as supported by the impedance analysis. The Nyquist plot derived from EIS measurements depicts the usual features of capacitive materials, ie x-intercept at high frequency region due to the equivalent series resistance of the cell (R_s), a semicircle at high-medium frequency region, followed by the Warburg region at medium frequencies and a vertical line at low frequencies. The slope of the Warburg region is connected to the electrical distributed resistance (Z_d) of the porous electrode [90], while the semicircle resistance (the closure point of the circle as real resistance increases in the Nyquist plot) is related to the combination of the electrical conductivity of the electrode, the ion diffusion resistance of the electrolyte in the pores and the bulk capacitance of the electrolyte (charge transfer resistance, R_{ct}) [91]. The values of the different resistances are compiled in Table S1. It is found that the values of Z_d and R_s

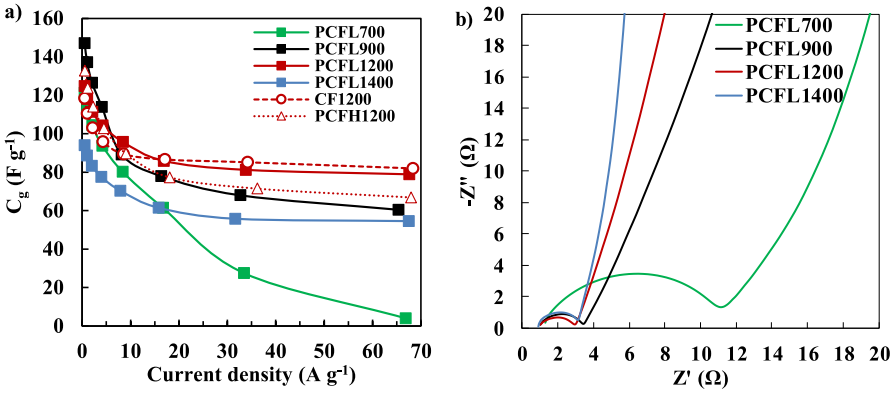

Fig. 9. a) Rate performance of CF1200, PCFH1200 and PCFL series. Current density between 0.5 and 68 A g^{-1} b) Nyquist plot derived from the EIS measurements of PCFL series. (A colour version of this figure can be viewed online.)

decreases with the carbonization temperature, as visually confirmed in Fig. 9b, and they are further decreased after the heat treatments. This improvement is undoubtedly related to the increase in electrical conductivity with the preparation temperature of the electrode, Table 5. Differently, the one related to the ion diffusion resistance, R_{CT}, registers an increase at 1400 °C, due to the presence of higher ion diffusional constraints, which are imposed by the shrinkage of the microporosity. This result explains why this material showed a slightly lower capacitance retention than PCFL1200, Fig. 9. a. The slope of the Nyquist plot in the medium to low frequency region can be also connected to the presence of pseudocapacitance in carbon materials [92]. In agreement with the CV responses and the capacitance retention test, PCFL1400 shows almost vertical line in this region, evidencing the almost pure capacitive response of this sample. In clear contrast, PCFL900 and PCFL700 shows slightly tilted lines for this region, related to the progressive loss of the contribution of slow surface redox reactions to the capacitance of the electrode as the frequency of the test increases.

4. Conclusions

Porous carbon fibers were prepared by carbonization of pure and phosphorus-functionalized electrospun lignin fibers at temperatures between 500 and 900 °C followed by thermal treatments from 1200 to 1600 °C. The incorporation of phosphoric acid in the lignin solution during the electrospinning show several advantages, namely: i) faster air stabilization stage ii) increase of carbonization and preparation yields iii) generation of stable oxygen and phosphorus groups iv) preservation of large porosity development and high electrical conductivity after thermal annealing at 1600 °C v) increase of the gravimetric capacitance and surface wettability for aqueous electrolytes.

XPS, TPD and ICP measurements revealed the presence of stable oxidized phosphorus groups in the carbonized H_3PO_4-containing lignin fibers. These groups remain linked to the surface after the thermal treatment at 1200 °C, where the phosphorus amount reaches a maximum value of 3% wt. Thermal treatments at higher temperatures produces the devolatilization of surface phosphorus. However, XPS depth profiling and ICP revealed the presence of reduced phosphorus in the core of the fibers treated at 1600 °C.

Microporosity is developed as carbonization temperature increases for pure carbon fibers, showing A_{BET} vale of 800 $m^2\ g^{-1}$ at 900 °C. The addition of phosphoric acid to the electrospinning solution increases the microporosity development, obtaining more than 1100 $m^2\ g^{-1}$ when a H_3PO_4 to lignin mass ratio of 0.3 is used. The thermal treatment at 1600 °C produce a marked shrinkage of the wide microporosity in pure carbon fibers. However, phosphorus-functionalized carbon fibers maintain most of their microporosity, showing A_{BET} values higher than 800 $m^2\ g^{-1}$ at the same temperature. XRD and Raman analyses confirm that the thermal treatment increases the structural order of both pure and phosphorus-functionalized carbon fibers, showing similar growing of the lateral size of the carbon microcrystallites. TEM and XRD analysis make evident that the presence of phosphorus in the core of the fibers induces curvature of the graphitic layers, which seems to hinder the stacking of the graphene layers, explaining the preservation of microporosity after the thermal treatment at high temperature by preventing the collapse of the micropores in those samples. Nevertheless, since the presence of phosphorus does not affect the lateral growing of the microcrystallites, the relatively high porosity does not compromise the electrical conductivity of P-containing carbon fibers, which shows a 2-fold increase after the heat treatment at the highest temperature.

Cyclic voltammetry measurements in acid electrolyte reveal a generalized improvement of gravimetric capacitance and wettability of carbonized and heat-treated fibers is observed by using a very low H_3PO_4 to lignin mass ratio of 0.1. Capacitance retention of ca. 65% when current density is 128-fold increased has been determined for the P-containing sample heat treated at 1200 °C. In addition, the enhanced electrical conductivity attained by P-containing carbon fibers at 700 °C allow their use as a capacitive material.

In sum, the high structural order, electrical conductivity and porosity development of electrospun lignin-based functional carbon fibers make them a promising candidate for advanced energy conversion and storage applications, such as supercapacitors and fuel cells.

CRediT authorship contribution statement

Francisco J. García-Mateos: Methodology, Investigation, Visualization, Writing – original draft. **Juana M. Rosas:** Visualization, Formal analysis, Supervision, Data curation, Writing – review & editing. **Ramiro Ruiz-Rosas:** Visualization, Formal analysis, Supervision, Data curation, Writing – review & editing. **José Rodríguez-Mirasol:** Conceptualization, Writing – review & editing, Funding acquisition, Project administration. **Tomás Cordero:** Conceptualization, Writing – review & editing, Funding acquisition, Project administration.

Declaration of competing interest

The authors declare that they have no known competing financial interests or personal relationships that could have appeared to influence the work reported in this paper.

Acknowledgments

We gratefully thank MICINN (RTI2018-097555-B-100) and Junta de Andalucía (UMA18-FEDERJA-110 and P18-RT-4592) for financial support.

Funding for open access charge: Universidad de Málaga / CBUA.

Appendix A. Supplementary data

Supplementary data to this article can be found online at https://doi.org/10.1016/j.carbon.2022.08.050.

References

[1] A.J. Ragauskas, G.T. Beckham, M.J. Biddy, R. Chandra, F. Chen, M.F. Davis, B. H. Davison, R.A. Dixon, P. Gilna, M. Keller, P. Langan, A.K. Naskar, J.N. Saddler, T. J. Tschaplinski, G.A. Tuskan, C.E. Wyman, Lignin valorization: improving lignin processing in the biorefinery, Science 344 (2014), 1246843, https://doi.org/10.1126/science.1246843.

[2] R. Rinaldi, R. Jastrzebski, M.T. Clough, J. Ralph, M. Kennema, P.C.A. Bruijnincx, B. M. Weckhuysen, Paving the way for lignin valorisation: recent advances in bioengineering, biorefining and catalysis, Angew. Chem. Int. Ed. 55 (2016) 8164–8215, https://doi.org/10.1002/anie.201510351.

[3] J.M. Rosas, R. Berenguer, M.J. Valero-Romero, J. Rodríguez-Mirasol, T. Cordero, Preparation of different carbon materials by thermochemical conversion of lignin, Front. Mater. 1 (2014) 29, https://doi.org/10.3389/fmats.2014.00029.

[4] C. Li, X. Zhao, A. Wang, G.W. Huber, T. Zhang, Catalytic transformation of lignin for the production of chemicals and fuels, Chem. Rev. 115 (2015) 11559–11624, https://doi.org/10.1021/acs.chemrev.5b00155.

[5] P. Fatehi, Extraction of technical lignins from pulping spent liquors, challenges and opportunities, in: Z. Fang, R.L. Smith Jr. (Eds.), Production of Biofuels and Chemicals from Lignin, Springer, Singapore, 2016, pp. 35–54, https://doi.org/10.1007/978-981-10-1965-4_8.

[6] J.J. Rodríguez, T. Cordero, J. Rodríguez-Mirasol, Carbon materials from lignin and their applications, in: Z. Fang, R.L. Smith Jr. (Eds.), Production of Biofuels and Chemicals from Lignin, Springer Singapore, Singapore, 2016, pp. 217–262, https://doi.org/10.1007/978-981-10-1965-4_8.

[7] A.M. Puziy, O.I. Poddubnaya, O. Sevastyanova, Carbon Materials from Technical Lignins : Recent Advances, Springer International Publishing, 2018, https://doi.org/10.1007/s41061-018-0210-7.

[8] J. Rodriguez-Mirasol, T. Cordero, L.R. Radovic, J.J. Rodriguez, Structural and textural properties of pyrolytic carbon formed within a microporous zeolite template, Chem. Mater. 10 (1998) 550–558, https://doi.org/10.1021/cm970552p.

[9] E. Gonzalez-Serrano, T. Cordero, J. Rodriguez-Mirasol, L. Cotoruelo, J. J. Rodriguez, Removal of water pollutants with activated carbons prepared from H 3PO4 activation of lignin from kraft black liquors, Water Res. 38 (2004) 3043–3050, https://doi.org/10.1016/j.watres.2004.04.048.

[10] M.J. Valero-Romero, E.M. Márquez-Franco, J. Bedia, J. Rodríguez-Mirasol, T. Cordero, Hierarchical porous carbons by liquid phase impregnation of zeolite templates with lignin solution, Microporous Mesoporous Mater. 196 (2014) 68–78, https://doi.org/10.1016/j.micromeso.2014.04.055.

[11] M. Lallave, J. Bedia, R. Ruiz-Rosas, J. Rodríguez-Mirasol, T. Cordero, J.C. Otero, M. Marquez, A. Barrero, I.G. Loscertales, Filled and hollow carbon nanofibers by coaxial electrospinning of Alcell lignin without binder polymers, Adv. Mater. 19 (2007) 4292–4296, https://doi.org/10.1002/adma.200700963.

[12] J. Rodríguez-Mirasol, T. Cordero, J.J. Rodríguez, High-temperature carbons from kraft lignin, Carbon 34 (1996) 43–52, https://doi.org/10.1016/0008-6223(95)00133-6.

[13] D.A. Baker, T.G. Rials, Recent advances in low-cost carbon fiber manufacture from lignin, J. Appl. Polym. Sci. 130 (2013) 713–728, https://doi.org/10.1002/app.39273.

[14] D.J. Johnson, I. Tomizuka, O. Watanabe, The fine structure of lignin-based carbon fibres, Carbon 13 (1975) 321–325, https://doi.org/10.1016/0008-6223(75)90037-8.

[15] D.A. Baker, N.C. Gallego, F.S. Baker, On the characterization and spinning of an organic-purified lignin toward the manufacture of low-cost carbon fiber, J. Appl. Polym. Sci. 124 (2012) 227–234, https://doi.org/10.1002/app.33596.

[16] A.L. Compere, W.L. Griffith, C.F. Leitten Jr., J.T. Shaffer, Low cost carbon fiber from renewable resources, in: International SAMPE Technical Conference, 2001, pp. 1306–1314.

[17] R. Ruiz-Rosas, J. Bedia, M. Lallave, I.G. Loscertales, A. Barrero, J. Rodríguez-Mirasol, T. Cordero, The production of submicron diameter carbon fibers by the electrospinning of lignin, Carbon 48 (2010) 696–705, https://doi.org/10.1016/j.carbon.2009.10.014.

[18] R. Berenguer, F.J. García-Mateos, R. Ruiz-Rosas, D. Cazorla-Amorós, E. Morallón, J. Rodríguez-Mirasol, T. Cordero, Biomass-derived binderless fibrous carbon electrodes for ultrafast energy storage, Green Chem. 18 (2016) 1506–1515.

[19] F.J. García-Mateos, T. Cordero-Lanzac, R. Berenguer, E. Morallón, D. Cazorla-Amorós, J. Rodríguez-Mirasol, T. Cordero, Lignin-derived Pt supported carbon (submicron)fiber electrocatalysts for alcohol electro-oxidation, Appl. Catal. B Environ. 211 (2017) 18–30, https://doi.org/10.1016/j.apcatb.2017.04.008.

[20] F.J. García-Mateos, R. Berenguer, M.J. Valero-Romero, J. Rodríguez-Mirasol, T. Cordero, Phosphorus functionalization for the rapid preparation of highly nanoporous submicron-diameter carbon fibers by electrospinning of lignin solutions, J. Mater. Chem. A. 6 (2018) 1219–1233, https://doi.org/10.1039/C7TA08788H.

[21] F.J. García-Mateos, R. Ruiz-Rosas, J. María Rosas, E. Morallón, D. Cazorla-Amorós, J. Rodríguez-Mirasol, T. Cordero, Activation of electrospun lignin-based carbon fibers and their performance as self-standing supercapacitor electrodes, Separ. Purif. Technol. 241 (2020), 116724, https://doi.org/10.1016/j.seppur.2020.116724.

[22] F.J. García-Mateos, R. Ruiz-Rosas, J.M. Rosas, J. Rodríguez-Mirasol, T. Cordero, Phosphorus containing carbon (submicron)fibers as efficient acid catalysts, Catal. Today 383 (2022) 308–319, https://doi.org/10.1016/j.cattod.2020.10.025.

[23] M. Zhu, H. Liu, Q. Cao, H. Zheng, D. Xu, H. Guo, S. Wang, Y. Li, J. Zhou, Electrospun lignin-based carbon nanofibers as supercapacitor electrodes, ACS Sustainable Chem. Eng. 8 (2020) 12831–12841, https://doi.org/10.1021/acssuschemeng.0c03062.

[24] H. Liu, T. Xu, K. Liu, M. Zhang, W. Liu, H. Li, H. Du, C. Si, Lignin-based electrodes for energy storage application, Ind. Crop. Prod. 165 (2021), 113425, https://doi.org/10.1016/j.indcrop.2021.113425.

[25] H. Zheng, Q. Cao, M. Zhu, D. Xu, H. Guo, Y. Li, J. Zhou, Biomass-based flexible nanoscale carbon fibers: effects of chemical structure on energy storage properties, J. Mater. Chem. A. 9 (2021) 10120–10134, https://doi.org/10.1039/D1TA00317H.

[26] M. Zhou, A. Bahi, Y. Zhao, L. Lin, F. Ko, P. Servati, S. Soltanian, P. Wang, Y. Yu, Q. Wang, Z. Cai, Enhancement of charge transport in interconnected lignin-derived carbon fibrous network for flexible battery-supercapacitor hybrid device, Chem. Eng. J. 409 (2021), 128214, https://doi.org/10.1016/j.cej.2020.128214.

[27] J.M. Rosas, J. Bedia, J. Rodriguez-Mirasol, T. Cordero, Preparation of hemp-derived activated carbon monoliths. Adsorption of water vapor, Ind. Eng. Chem. Res. 47 (2008) 1288–1296, https://doi.org/10.1021/ie070924w.

[28] M.J. Valero-Romero, F.J. García-Mateos, J. Rodríguez-Mirasol, T. Cordero, Role of surface phosphorus complexes on the oxidation of porous carbons, Fuel Process. Technol. 157 (2017) 116–126, https://doi.org/10.1016/j.fuproc.2016.11.014.

[29] M. Jagtoyen, F. Derbyshire, Activated carbons from yellow poplar and white oak by H3PO4 activation, Carbon 36 (1998) 1085–1097, https://doi.org/10.1016/S0008-6223(98)00082-7.

[30] J.M. Rosas, J. Bedia, J. Rodríguez-Mirasol, T. Cordero, HEMP-derived activated carbon fibers by chemical activation with phosphoric acid, Fuel 88 (2009) 19–26, https://doi.org/10.1016/j.fuel.2008.08.004.

[31] S. Kubo, Y. Uraki, Y. Sano, Preparation of carbon fibers from softwood lignin by atmospheric acetic acid pulping, Carbon 36 (1998) 1119–1124, https://doi.org/10.1016/S0008-6223(98)00086-4.

[32] F.J. García-Mateos, R. Ruiz-Rosas, M.D. Marqués, L.M. Cotoruelo, J. Rodríguez-Mirasol, T. Cordero, Removal of paracetamol on biomass-derived activated carbon: modeling the fixed bed breakthrough curves using batch adsorption experiments, Chem. Eng. J. 279 (2015) 18–30, https://doi.org/10.1016/j.cej.2015.04.144.

[33] A.M. Puziy, O.I. Poddubnaya, A. Martínez-Alonso, F. Suárez-García, J.M.D. Tascón, Surface chemistry of phosphorus-containing carbons of lignocellulosic origin, Carbon 43 (2005) 2857–2868, https://doi.org/10.1016/j.carbon.2005.06.014.

[34] J.M. Rosas, R. Ruiz-Rosas, J. Rodríguez-Mirasol, T. Cordero, Kinetic study of the oxidation resistance of phosphorus-containing activated carbons, Carbon 50 (2012) 1523–1537, https://doi.org/10.1016/j.carbon.2011.11.030.

[35] F. Tuinstra, J.L. Koenig, Raman spectrum of graphite, J. Chem. Phys. 53 (1970) 1126–1130, https://doi.org/10.1063/1.1674108.

[36] M. Nakamizo, R. Kammereck, P.L. Walker, Laser Raman studies on carbons, Carbon 12 (1974) 259–267, https://doi.org/10.1016/0008-6223(74)90068-2.

[37] P. Lespade, A. Marchand, M. Couzi, F. Cruege, Caracterisation de materiaux carbones par microspectrometrie Raman, Carbon 22 (1984) 375–385, https://doi.org/10.1016/0008-6223(84)90009-5.

[38] Y.-J. Lee, The second order Raman spectroscopy in carbon crystallinity, J. Nucl. Mater. 325 (2004) 174–179, https://doi.org/10.1016/j.jnucmat.2003.12.005.

[39] A.C. Ferrari, J.C. Meyer, V. Scardaci, C. Casiraghi, M. Lazzeri, F. Mauri, S. Piscanec, D. Jiang, K.S. Novoselov, S. Roth, A.K. Geim, Raman spectrum of graphene and graphene layers, Phys. Rev. Lett. 97 (2006), 187401, https://doi.org/10.1103/PhysRevLett.97.187401.

[40] D.S. Knight, W.B. White, Characterization of diamond films by Raman spectroscopy, J. Mater. Res. 4 (1989) 385–393, https://doi.org/10.1557/JMR.1989.0385.

[41] A. Cuesta, P. Dhamelincourt, J. Laureyns, A. Martínez-Alonso, J.M.D. Tascón, Raman microprobe studies on carbon materials, Carbon 32 (1994) 1523–1532, https://doi.org/10.1016/0008-6223(94)90148-1.

[42] A. Sadezky, H. Muckenhuber, H. Grothe, R. Niessner, U. Pöschl, Raman microspectroscopy of soot and related carbonaceous materials: spectral analysis and structural information, Carbon 43 (2005) 1731–1742, https://doi.org/10.1016/j.carbon.2005.02.018.

[43] A.W.P. Fung, A.M. Rao, K. Kuriyama, M.S. Dresselhaus, G. Dresselhaus, M. Endo, N. Shindo, Raman scattering and electrical conductivity in highly disordered activated carbon fibers, J. Mater. Res. 8 (1993) 489–500, https://doi.org/10.1557/JMR.1993.0489.

[44] G.K. Gueorguiev, A. Furlan, H. Högberg, S. Stafström, L. Hultman, First-principles calculations on the structural evolution of solid fullerene-like CPx, Chem. Phys. Lett. 426 (2006) 374–379, https://doi.org/10.1016/j.cplett.2006.05.087.

[45] A. Furlan, G.K. Gueorguiev, H. Högberg, S. Stafström, L. Hultman, Fullerene-like CPx: a first-principles study of the relative stability of precursors and defect energetics during synthetic growth, Thin Solid Films 515 (2006) 1028–1032, https://doi.org/10.1016/j.tsf.2006.07.176.

[46] S. Melchor, J.A. Dobado, J.A. Larsson, J.C. Greer, Bonding of atomic phosphorus to polycyclic hydrocarbons and curved graphitic surfaces, J. Am. Chem. Soc. 125 (2003) 2301–2306, https://doi.org/10.1021/ja027520+.

[47] A. Furlan, G.K. Gueorguiev, Zs Czigány, H. Högberg, S. Braun, S. Stafström, L. Hultman, Synthesis of phosphorus-carbide thin films by magnetron sputtering, Phys. Status Solidi Rapid Res. Lett. 2 (2008) 191–193, https://doi.org/10.1002/pssr.200802077.

[48] G.K. Gueorguiev, Zs Czigány, A. Furlan, S. Stafström, L. Hultman, Intercalation of P atoms in fullerene-like CPx, Chem. Phys. Lett. 501 (2011) 400–403, https://doi.org/10.1016/j.cplett.2010.11.024.

[49] J. Bedia, J.M. Rosas, J. Márquez, J. Rodríguez-Mirasol, T. Cordero, Preparation and characterization of carbon based acid catalysts for the dehydration of 2-propanol, Carbon 47 (2009) 286–294, https://doi.org/10.1016/j.carbon.2008.10.008.

[50] A.M. Rao, A.W.P. Fung, M.S. Dresselhaus, M. Endo, Structural characterization of heat-treated activated carbon fibers, J. Mater. Res. 7 (1992) 1788–1794, https://doi.org/10.1557/JMR.1992.1788.

[51] S. Hu, S. Zhang, N. Pan, Y.-L. Hsieh, High energy density supercapacitors from lignin derived submicron activated carbon fibers in aqueous electrolytes, J. Power Sources 270 (2014) 106–112, https://doi.org/10.1016/j.jpowsour.2014.07.063.

[52] Y. Zhao, Y. Liu, C. Tong, J. Ru, B. Geng, Z. Ma, H. Liu, L. Wang, Flexible lignin-derived electrospun carbon nanofiber mats as a highly efficient and binder-free counter electrode for dye-sensitized solar cells, J. Mater. Sci. 53 (2018) 7637–7647, https://doi.org/10.1007/s10853-018-2059-0.

[53] M. Janani, P. Srikrishnarka, S.V. Nair, A.S. Nair, An in-depth review on the role of carbon nanostructures in dye-sensitized solar cells, J. Mater. Chem. A. 3 (2015) 17914–17938, https://doi.org/10.1039/C5TA03644E.

[54] A. Lund, N.M. van der Velden, N.-K. Persson, M.M. Hamedi, C. Müller, Electrically conducting fibres for e-textiles: an open playground for conjugated polymers and carbon nanomaterials, Mater. Sci. Eng. R Rep. 126 (2018) 1–29, https://doi.org/10.1016/j.mser.2018.03.001.

[55] H. Tang, C.M. Hessel, J. Wang, N. Yang, R. Yu, H. Zhao, D. Wang, Two-dimensional carbon leading to new photoconversion processes, Chem. Soc. Rev. 43 (2014) 4281–4299, https://doi.org/10.1039/c3cs60437c.

[56] M.R. Snowdon, A.K. Mohanty, M. Misra, A study of carbonized lignin as an alternative to carbon black, ACS Sustainable Chem. Eng. 2 (2014) 1257–1263, https://doi.org/10.1021/sc500086v.

[57] F. Beguin, E. Frackowiak, Carbons for Electrochemical Energy Storage and Conversion Systems, CRC Press, Boca Raton, 2010.

[58] F. Quesada-Plata, R. Ruiz-Rosas, E. Morallón, D. Cazorla-Amorós, Activated carbons prepared through H3PO4-assisted hydrothermal carbonisation from biomass wastes: porous texture and electrochemical performance, ChemPlusChem 81 (2016) 1349–1359, https://doi.org/10.1002/cplu.201600412.

[59] K.H. Radeke, K.O. Backhaus, A. Swiatkowski, Electrical conductivity of activated carbons, Carbon 29 (1991) 122–123, https://doi.org/10.1016/0008-6223(91)90103-.

[60] L. Soukup, I. Gregora, L. Jastrabik, A. Koňáková, Raman spectra and electrical conductivity of glassy carbon, Mater. Sci. Eng., B 11 (1992) 355–357, https://doi.org/10.1016/0921-5107(92)90240-A.

[61] D. Pantea, H. Darmstadt, S. Kaliaguine, L. Sümmchen, C. Roy, Electrical conductivity of thermal carbon blacks: influence of surface chemistry, Carbon 39 (2001) 1147–1158, https://doi.org/10.1016/S0008-6223(00)00239-6.

[62] S.L. di Vittorio, M.S. Dresselhaus, M. Endo, J.-P. Issi, L. Piraux, V. Bayot, The transport properties of activated carbon fibers, J. Mater. Res. 6 (1991) 778–783, https://doi.org/10.1557/JMR.1991.0778.

[63] N.-Y. Teng, I. Dallmeyer, J.F. Kadla, Incorporation of multiwalled carbon nanotubes into electrospun softwood kraft lignin-based fibers, J. Wood Chem. Technol. 33 (2013) 299–316, https://doi.org/10.1080/02773813.2013.795807.
[64] X. Wang, Y. Zhu, X. Wang, G. Liu, J. Li, R. Zhao, Y. Zhang, X. Zhang, G. Han, H. Zhao, J. Yu, In-situ growth of graphene on carbon nanofiber from lignin, Carbon 169 (2020) 446–454, https://doi.org/10.1016/j.carbon.2020.07.070.
[65] J.S. Im, S.C. Kang, S.-H. Lee, Y.-S. Lee, Improved gas sensing of electrospun carbon fibers based on pore structure, conductivity and surface modification, Carbon 48 (2010) 2573–2581, https://doi.org/10.1016/j.carbon.2010.03.045.
[66] H. Li, D. Yuan, C. Tang, S. Wang, J. Sun, Z. Li, T. Tang, F. Wang, H. Gong, C. He, Lignin-derived interconnected hierarchical porous carbon monolith with large areal/volumetric capacitances for supercapacitor, Carbon 100 (2016) 151–157, https://doi.org/10.1016/j.carbon.2015.12.075.
[67] R. Berenguer, F.J. García-Mateos, R. Ruiz-Rosas, D. Cazorla-Amorós, E. Morallón, J. Rodríguez-Mirasol, T. Cordero, Biomass-derived binderless fibrous carbon electrodes for ultrafast energy storage, Green Chem. 18 (2016) 1506–1515, https://doi.org/10.1039/C5GC02409A.
[68] P. Schlee, O. Hosseinaei, D. Baker, A. Landmér, P. Tomani, M.J. Mostazo-López, D. Cazorla-Amorós, S. Herou, M.-M. Titirici, From waste to wealth: from kraft lignin to free-standing supercapacitors, Carbon 145 (2019) 470–480, https://doi.org/10.1016/j.carbon.2019.01.035.
[69] M.J. Bleda-Martínez, J.A. Maciá-Agulló, D. Lozano-Castelló, E. Morallón, D. Cazorla-Amorós, A. Linares-Solano, Role of surface chemistry on electric double layer capacitance of carbon materials, Carbon 43 (2005) 2677–2684, https://doi.org/10.1016/j.carbon.2005.05.027.
[70] K. Nueangnoraj, R. Ruiz-Rosas, H. Nishihara, S. Shiraishi, E. Morallón, D. Cazorla-Amorós, T. Kyotani, Carbon–carbon asymmetric aqueous capacitor by pseudocapacitive positive and stable negative electrodes, Carbon 67 (2014) 792–794, https://doi.org/10.1016/j.carbon.2013.10.011.
[71] L. Eliad, G. Salitra, A. Soffer, D. Aurbach, Ion sieving effects in the electrical double layer of porous carbon electrodes: estimating effective ion size in electrolytic solutions, J. Phys. Chem. B 105 (2001) 6880–6887, https://doi.org/10.1021/jp010086y.
[72] B. Lobato, L. Suárez, L. Guardia, T.A. Centeno, Capacitance and surface of carbons in supercapacitors, Carbon 122 (2017) 434–445, https://doi.org/10.1016/j.carbon.2017.06.083.
[73] S. Zhao, Z. Song, L. Qing, J. Zhou, C. Qiao, Surface wettability effect on energy density and power density of supercapacitors, J. Phys. Chem. C 126 (2022) 9248–9256, https://doi.org/10.1021/acs.jpcc.2c01455.
[74] R. Ruiz-Rosas, E. Bohórquez-Guarín, D. Cazorla-Amorós, E. Morallón, Role of heteroatoms on the performance of porous carbons as electrode in electrochemical, in: Innovations in Engineered Porous Materials for Energy Generation and Storage Applications, CRC Press, Taylor & Francis group, 2018, pp. 109–142.
[75] S.I. Yun, S.H. Kim, D.W. Kim, Y.A. Kim, B.-H. Kim, Facile preparation and capacitive properties of low-cost carbon nanofibers with ZnO derived from lignin and pitch as supercapacitor electrodes, Carbon 149 (2019) 637–645, https://doi.org/10.1016/j.carbon.2019.04.105.
[76] P. Schlee, O. Hosseinaei, C.A.O. Keefe, M.J. Mostazo-López, D. Cazorla-Amorós, S. Herou, P. Tomani, C.P. Grey, M.-M. Titirici, Hardwood versus softwood Kraft lignin – precursor-product relationships in the manufacture of porous carbon nanofibers for supercapacitors, J. Mater. Chem. A. 8 (2020) 23543–23554, https://doi.org/10.1039/D0TA09093J.
[77] J. Chmiola, G. Yushin, Y. Gogotsi, C. Portet, P. Simon, P.L. Taberna, Anomalous increase in carbon capacitance at pore sizes less than 1 nanometer, Science 313 (2006) 1760–1763, https://doi.org/10.1126/science.1132195.
[78] C. Largeot, C. Portet, J. Chmiola, P.-L. Taberna, Y. Gogotsi, P. Simon, Relation between the ion size and pore size for an electric double-layer capacitor, J. Am. Chem. Soc. 130 (2008) 2730–2731, https://doi.org/10.1021/ja7106178.
[79] D. Cazorla-Amorós, J. Alcañiz-Monge, M.A. de la Casa-Lillo, A. Linares-Solano, CO2 as an adsorptive to characterize carbon molecular sieves and activated carbons, Langmuir 14 (1998) 4589–4596, https://doi.org/10.1021/la980198p.
[80] M.J. Bleda-Martínez, D. Lozano-Castelló, E. Morallón, D. Cazorla-Amorós, A. Linares-Solano, Chemical and electrochemical characterization of porous carbon materials, Carbon 44 (2006) 2642–2651, https://doi.org/10.1016/j.carbon.2006.04.017.
[81] L.R. Radovic, Surface chemical and electrochemical properties of carbons, in: F. Beguin, E. Frackowiak (Eds.), Carbons for Electrochemical Energy Storage and Conversion Systems, Taylor & Francis (CRC Press), Boca Raton, FL, 2010, pp. 163–219.
[82] C. Huang, T. Sun, D. Hulicova-Jurcakova, Wide electrochemical window of supercapacitors from coffee bean-derived phosphorus-rich carbons, ChemSusChem 6 (2013) 2330–2339, https://doi.org/10.1002/cssc.201300457.
[83] R. Berenguer, R. Ruiz-Rosas, A. Gallardo, D. Cazorla-Amorós, E. Morallón, H. Nishihara, T. Kyotani, J. Rodríguez-Mirasol, T. Cordero, Enhanced electro-oxidation resistance of carbon electrodes induced by phosphorus surface groups, Carbon 95 (2015) 681–689, https://doi.org/10.1016/j.carbon.2015.08.101.
[84] D. Yu, Q. Qian, L. Wei, W. Jiang, K. Goh, J. Wei, J. Zhang, Y. Chen, Emergence of fiber supercapacitors, Chem. Soc. Rev. 44 (2015) 647–662, https://doi.org/10.1039/C4CS00286E.
[85] Y. Wang, J. Cui, Q. Qu, W. Ma, F. Li, W. Du, K. Liu, Q. Zhang, S. He, C. Huang, Free-standing porous carbon nanofiber membranes obtained by one-step carbonization and activation for high-performance supercapacitors, Microporous Mesoporous Mater. 329 (2022), 111545, https://doi.org/10.1016/j.micromeso.2021.111545.
[86] W. Xu, Y. Lu, H. Chi, H. Zhao, J. Hu, G. Xiao, Boosted electrochemical properties of polyimide-based carbon nanofibers containing micro/mesopore for high-performance supercapacitors by thermal rearrangement, J. Energy Storage 47 (2022), https://doi.org/10.1016/j.est.2021.103672, 103672.
[87] J. Jia, Z. Qin, X. Yang, B. Gu, M. Yin, Z. Lin, Electrospun carbon nanofibers from PAN and a loose medium component of coal as binder-free electrodes for supercapacitors, J. Taiwan Inst. Chem. Eng. 132 (2022), 104233, https://doi.org/10.1016/j.jtice.2022.104233.
[88] X. Li, Y. Li, X. Tian, Y. Song, Y. Cui, Flexible and cross-linked carbon nanofibers based on coal liquefaction residue for high rate supercapacitors, J. Alloys Compd. 903 (2022), 163919, https://doi.org/10.1016/j.jallcom.2022.163919.
[89] H.C. Lee, Y.A. Kim, B.-H. Kim, Electrochemical activity of triple-layered boron-containing carbon nanofibers with hollow channels in supercapacitors, Carbon 196 (2022) 78–84, https://doi.org/10.1016/j.carbon.2022.04.061.
[90] R. Kötz, M. Carlen, Principles and applications of electrochemical capacitors, Electrochim. Acta 45 (2000) 2483–2498, https://doi.org/10.1016/S0013-4686(00)00354-6.
[91] S. Fletcher, V.J. Black, I. Kirkpatrick, A universal equivalent circuit for carbon-based supercapacitors, J. Solid State Electrochem. 18 (2013) 1377–1387, https://doi.org/10.1007/s10008-013-2328-4.
[92] B.E. Conway, Electrochemical Supercapacitors: Scientific Fundamentals and Technological Applications, Kluwer-Plenum Press, New York, 1999.